UNIVERSITY OF COPENHAGEN
FACULTY OF SCIENCE (DEPARTMENT OF FOOD AND RESOURCE ECONOMICS)

Master of Science (MSc) in Global Forestry (GLOFOR)

Multi-Seasonal Remote Sensing-Based Aboveground Biomass Estimation in Nepal: A Case Study in Kankali Community Forest

Date: 15 August 2025

Supervisor
Henrik Meilby
Professor
Department of Food and Resource Economics, UCPH

Co-Supervisor
Sony Baral
Associate Professor
Tribhuvan University

Author
Pooja Regmi
Student No. bjm779

Abstract

Accurate above-ground biomass (AGB) estimation supports sustainable forest management, carbon accounting, and climate mitigation. This study evaluated Landsat-derived vegetation indices (NDVI, EVI, NBR) from different seasonal windows with linear, quadratic, and Random Forest models to estimate AGB in Nepal's Kankali Community Forest using field data from 2005–2025. Biomass increased substantially over two decades, reflecting effective community forestry management. Post-monsoon (November) indices, particularly EVI, exhibited the strongest correlations with AGB, while dry season (March) indices showed weakened relationships. Among the tested models, the Random Forest algorithm with November-only vegetation indices achieved the highest overall accuracy in this study (test $R^2 = 0.66$, RMSE = 79.49), marginally ahead of multi-season data ($R^2 = 0.62$). Incorporating elevation and coarse climate variables produced negligible accuracy gains, likely due to the site's narrow environmental gradients and the strong predictive power of spectral indices alone. Findings confirm the value of optimally timed optical imagery and robust nonlinear models for scalable biomass monitoring, with clear application potential for REDD+, forest inventories, and carbon stock assessment in similar lowland tropical systems.

Keywords: aboveground biomass, remote sensing, Landsat, multi-seasonal, vegetation indices

Acknowledgements

I would like to express my deepest gratitude to my supervisor, Professor Henrik Meilby, Department of Food and Resource Economics, University of Copenhagen, for his unwavering guidance, constructive feedback, and encouragement throughout the course of this thesis. His extensive experience with the Kankali Community Forest and insightful perspectives have been invaluable in shaping both the methodological approach and the overall quality of this work.

I am also grateful to my co-supervisor, Associate Professor Sony Baral, Tribhuvan University, whose expertise and prior research in the same forest provided essential direction and support. Her thoughtful advice and readiness to assist at every stage greatly enriched this study.

My sincere thanks go to the Institute of Forestry, Tribhuvan University, for granting access to the historical temporal data of the Kankali Community Forest, which served as a crucial foundation for this research. I also wish to acknowledge the Kankali Community Forest for allowing access to the study site and for facilitating fieldwork by providing skilled inventory personnel to assist with data collection. In particular, I am grateful to Keshav Ayer, Hemant Joshi, and Rojit for their dedicated support in data collection and their valuable assistance throughout the research process.

Finally, I would like to extend my appreciation to the University of Copenhagen for enabling this master's thesis and for providing an excellent academic environment in which to pursue my studies.

To all who have contributed their time, knowledge, and support, whether in the field, in the office, or from afar, please accept my heartfelt thanks.

Table of Contents

List of Figures and Tables

Figures

Tables

List of Abbreviations and Acronyms

Abbreviation	Definition
AGB	Above-Ground Biomass
CF	Community Forest
ComForM	Community-based Forestry in the Nepal Himalaya
CRU CY	Climatic Research Unit Climate Year
CRU TS	Climatic Research Unit gridded Time Series
CS	Carbon Stock
DBH	Diameter at Breast Height
EVI	Enhanced Vegetation Index
GEE	Google Earth Engine
GPS	Global Positioning System
LST	Land Surface Temperature
ML	Machine Learning
NDVI	Normalized Difference Vegetation Index
NBR	Normalized Burn Ratio
NIR	Near-Infrared
OLI	Operational Land Imager
PET	Potential Evapotranspiration
QA	Quality Assessment (as in QA_PIXEL)
REDD+	Reducing Emissions from Deforestation and Forest Degradation
RF	Random Forest
R^2	Coefficient of Determination
RMSE	Root Mean Square Error
RS	Remote Sensing
SR	Surface Reflectance
TM	Thematic Mapper
USGS	United States Geological Survey
VI/VIs	Vegetation Index/Vegetation Indices

1. Introduction

1.1. Background

Forests are essential to the global carbon cycle as they absorb carbon dioxide (CO_2) from the atmosphere and store it in various forms, including biomass, soil, deadwood, and litter (FAO, 2011). They hold about 80% of terrestrial carbon above ground and 40% below ground, acting as a significant buffer against climate change (Canadell & Raupach, 2008; Fahey et al., 2010; Pan et al., 2013). Forest carbon storage accounts for 82.5% of terrestrial vegetation carbon storage, which is the main component of the vegetation carbon sink (Kauranne et al., 2017). Through photosynthesis, forests operate as natural carbon sinks, with trees storing 43–50% of their dry biomass in carbon (Malhi et al., 2002). The above-ground biomass of a tree constitutes most of the carbon pool (K.C. et al., 2024). AGB is often defined as the dry weight of all aboveground live mass, including wood, bark, branches, twigs, and stumps (Dong et al., 2003). This is the most essential and visible carbon reserve in terrestrial forest ecosystems. Any changes in land-use systems, such as forest degradation and deforestation, pose a significant threat to this process, as they release stored carbon back into the atmosphere, increasing greenhouse gas (GHG) emissions and accelerating climate change (Vashum & Jayakumar, 2012).

The Kyoto Protocol was formulated in 1997 stating the principle that the soil and biomass can sequestrate CO2 from the air, which is one of the solutions for climate change (Harishma et al., 2020). Stopping deforestation alone will lead to a reduction of about 18% of atmospheric CO2 emissions (Khallaf, 2011), highlighting the crucial role that well-managed forests can play in global climate action. The Kyoto Protocol, Paris Agreement, and European Union Regulation (2018/841) emphasize the importance of estimating, documenting, and reporting carbon emissions and the extent of deforestation (UNFCCC, 2008, 2015; Forsell et al., 2018). Effective monitoring of forest biomass is crucial for meeting these international climate commitments.

Good estimation of forest biomass is crucial for various applications, including timber harvesting, calculation of forest carbon differences, and tracking the difference in the global carbon balance (K.C. et al., 2024). Above-ground biomass, in particular, is the most changeable and sensitive component of carbon storage, in the sense that it rapidly responds to people's management activities and the effect of global warming (Houghton et al., 2009). Forest biomass is estimated by using either a non-destructive or destructive method (Vashum & Jayakumar, 2012). Harvesting all trees in each sample area and measurement of the biomass of different parts is the destructive method (Ravindranath & Ostwald, 2007). It is costly, labor-intensive, and not feasible for the estimation on a large scale. Non-destructive methods include forest measurements combined with allometric equations to estimate biomass (Ismail et al., 2018). When executed with accuracy and comprehensiveness, forest inventories give reliable biomass and carbon estimates for the sampled areas (Ahmad et al., 2023). However, traditional inventory procedures are typically constrained by their high costs, massive labor requirements, and lack of spatial continuous coverage (Ahmad et al., 2023). Moreover, limitations such as inadequate access to the overall forested ecosystem and the inaccessibility of full quantitative information on forest degradation continue to influence effective biomass estimation.

Remote sensing techniques have become invaluable tools for vegetation mapping and ecological analysis by capturing the spectral reflectance characteristics of vegetation (Avitabile et al., 2012; Zhu & Liu, 2015). These approaches effectively address the limitations inherent in traditional forest inventories, which are often constrained in scope and scale (Sinha et al., 2015). The application of remote sensing (RS) for vegetation monitoring and mapping is now widely established and accepted within the scientific community (Ingram et al., 2005; Maynard et al., 2007; Lu et al., 2012). Since AGB cannot be directly measured from air or space, remote sensing methods rely on linking satellite-derived data with ground measurements. Various sensors have been utilized to map, monitor, and estimate forest biomass and carbon across different scales. Landsat images have been the most used medium-resolution data for estimating aboveground biomass (AGB) because they have the longest data record (since 1972) and a suitable spatial resolution (30 meters) for land management (Cohen & Goward, 2004; Lu et al., 2012; Main-Knorn et al., 2013). Among the various remote sensing models, those based on satellite-derived vegetation indices (VIs) are the most frequently employed for estimating above-ground biomass (Foody et al., 2003; Zheng et al., 2004; Almalki et al., 2022). Numerous studies have demonstrated a strong positive relationship between above-ground carbon stocks and different vegetation indices (Zheng et al., 2004; Maynard et al., 2007; Vicharnakorn et al., 2014). Consequently, VI-based models derived from satellite imagery are among the most commonly used and reliable approaches for analyzing, predicting, and estimating forest biomass at various scales (Ahmad et al., 2023; Zheng et al., 2004).

1.2. Rationale of the study

AGB has been measured to ensure that forest resources are maintained sustainably. As more world attention is brought to vegetation carbon sequestration, stimulated by protocols such as the United Nations Framework Convention on Climate Change (UNFCCC) and the Kyoto Protocol (Cheng et al., 2009), AGB estimation has become a vital tool for estimating deforestation effects and carbon sequestration ability. The integration of remote sensing and national forest inventories has improved the efficiency and precision of carbon stock estimation, reducing reliance on time-consuming field measurements (Zhu & Liu, 2015).

However, the many existing studies employed a single image of Landsat obtained in the peak growing period to derive models for predicting biomass. This is usually linked with saturation, in which the elevated AGB is underestimated, lowering the precision of models in closed forests (Zhu & Liu, 2015). In addition, although a number of studies utilized multi-temporal Landsat data, they typically utilized one image every year (Powell et al., 2010) or selected a single seasonally optimal image of the strongest correlation with AGB (Gasparri et al., 2010), which limited their ability to utilize full seasonal contrasts in vegetation reflectance. Dymond et al. (2002) highlighted that utilization of seasonal time-series images will significantly enhance the accuracy of forest attribute monitoring.

Furthermore, the challenge also remains in linking satellite observations and field measurements due to differences at various scales and differences in the time domain (Avitabile et al., 2012). The limitations highlight the potential for exploring utilization of seasonal Landsat time-series data further for enhancing AGB estimation accuracy as well as spatial resolution.

Given this need, this research examines the application of seasonal Landsat time-series for estimating:

1.3. Objective:

General Objective:

To improve the estimation of aboveground biomass in Kankali Community Forest by analyzing multi-seasonal remote sensing data and key environmental factors.

Specific Objectives

1. To quantify aboveground biomass changes in Kankali Community Forest between 2005 and 2025.
2. To identify the strongest vegetation index predictors (NDVI, EVI, NBR) for biomass estimation in post-monsoon and dry seasons.

3. To compare the performance of linear regression, quadratic regression, and Random Forest models for multi-seasonal biomass estimation and test whether topographic and climatic factors improve accuracy.

1.4. Research Questions

1. How has aboveground biomass in Kankali Community Forest changed over the past two decades?
2. Which vegetation indices (NDVI, EVI, NBR) and seasonal periods provide the strongest relationship with aboveground biomass?
3. Does using multi-seasonal vegetation indices improve the accuracy of AGB estimation models compared to using single-season imagery alone?
4. Does including topographic and climatic variables improve biomass estimation accuracy compared to vegetation indices alone?

1.5. Limitations

Remote Sensing and Modeling Constraints

1. In areas with steep terrain, topographic shadows, and illumination variations affect spectral reflectance, potentially inhibiting biomass estimation accuracy.
2. Multi-seasonal imagery was limited to post-monsoon (November) and dry season (March); other key phenological phases (e.g. pre-monsoon leaf flush or peak growing season) were not included.
3. The unavailability of November 2025 satellite imagery limited the temporal coverage of multi-seasonal analyses.

Ancillary Data Limitations

4. While elevation and country-level climate data were incorporated, local climate data were not available, possibly limiting the model's ability to capture fine-scale environmental influences on biomass.
5. Topographic data were restricted to elevation; other potentially relevant terrain metrics (e.g., slope, aspect, wetness indices) were not incorporated.
6. The number of sampled plots varied slightly across different years due to environmental disturbances, with some plots considered destroyed. However, biomass estimates were standardized per hectare to ensure comparability.

Data and Case Study Context

7. The study is based on a single community forest in Nepal, which limits direct generalization to other forest types, management regimes, or ecological zones. However, the results provide a valuable reference point for similar ecological zones and future research.
8. Field inventory data were collected at specific time intervals; any intra-annual biomass changes between these periods could not be captured.

2. Literature Review

2.1. Background and Significance of Aboveground Biomass Estimation

Forests serve as a global natural carbon reservoir, holding about 80% of the carbon in terrestrial above-ground biomass and 40% in below-ground biomass (Soto Navarro et al., 2020). Vegetation and soils serve as viable carbon sinks in the atmosphere and can make a considerable contribution to global climate change mitigation (Bajracharya et al., 2018). Forest carbon stock refers to the total quantity of carbon removed from the atmosphere and deposited in forest ecosystems as live biomass, soil carbon, deadwood, and litter (FAO, 2011). Carbon is often stored in biomass throughout the photosynthetic process (Alexandrov, 2007; Suryawanshi et al., 2014). And aboveground biomass (AGB) is a key factor influencing the functioning of a forest ecosystem (Behera et al., 2017). According to (Gibbs et al., 2007), the tree's above ground biomass is the greatest carbon pool.

Research on forest vegetation biomass is crucial for assessing carbon storage in the main tree components and understanding the carbon cycle at regional and global scales. Measuring the AGB of dominant tree species across various forest communities or plant functional types is particularly important, as these species significantly influence the scale and distribution of energy flow. This energy is stored in trunks, branches, leaves, and roots as organic substances and materials that continuously cycle between the biotic and abiotic components of the ecosystem. AGB levels in forests are determined by the differential between photosynthetic output and respiration consumption, as well as mortality, harvest, and herbivory (Behera et al., 2017). Estimating AGB is therefore an effective instrument for assessing both the structural and functional characteristics of forest ecosystems in a variety of environmental conditions (Brown et al., 1989; Ketterings et al., 2001)

There are two primary methodologies for estimating forest biomass: traditional field-based methods and remote sensing (RS) techniques. The traditional method estimates plot scale biomass by using tree-level biomass functions (often summing the biomass of all trees). Biomass for a specific area is then assessed using inventory plots, which vary based on the sampling method and intensity required to meet a specified error threshold, followed by an extrapolation process (Somogyi et al., 2007). Traditional procedures are time-consuming, difficult to deploy in remote areas (Lu, 2008; Henry et al., 2011). Remote sensing techniques, in contrast, have been increasingly popular since their inception. Over the past three decades, advancements in remote sensing technologies have made satellite images with diverse spectral, geographical, radiometric, and temporal resolutions widely accessible, enabling more efficient and scalable biomass estimation. Accurately estimating forest biomass can serve as an effective alternative to conventional forest monitoring systems and provides a critical foundation for evaluating ecosystem processes, ecosystem carbon balance, and the impacts of climate change (Zhu et al., 2020).

2.2. Vegetation Indices and Optical Remote Sensing in AGB Studies

Remote sensing allows the observation of the change detection of the forests and their biophysical parameters over varied scales through temporal analysis with comprehensive coverage which makes it one of the effective technologies in above-ground biomass (AGB) estimation (Sinha et al., 2015, Wang et al. 2022). The implementation of remote sensing in the evaluation of biomass has been more efficient and effective compared to the other traditional approaches of biomass estimation (Patenaude et al., 2005; Lu, 2006) due to the massive archive of freely available data for the biomass estimation (Patenaude et al., 2005; Avitabile et al., 2012; Du et al., 2012). Moreover, remote sensing can be used to assess the forest ecological processes as it deflects the limitations of traditional approaches of biomass estimation such as labor, time, and extensive cost through its geospatial features (Sinha et al., 2015, Li et al., 2020). In the AGB estimation, Landsat images have been commonly used medium-resolution data to date (Cutler et al., 2012; Du et al., 2012; Main-Knorn et al., 2013) due to the longest data recording feature of the Landsat (since 1972) with spatial resolution features (Cohen & Goward, 2004). Nevertheless, there is an ordinary problem with Landsat images, which data saturation is resulting in the decline of the accuracy of AGB assessment (Lu et al., 2016; Zhao et al., 2016) when AGB is higher than 130 Mg /ha (Lu et al., 2016). However, the AGB assessment can be improved using seasonal Landsat NDVI time series (Zhu & Liu, 2015).

Vegetation indices (VIs), which are acquired from sensing the earth coverings without physical contact, are considered simple mathematical procedures for assessing the coverage of vegetation, its strengths, and variation in the growth in different applications (Xue & Su, 2017). The mathematical groupings of reflectance bands of visible and near-infrared, as different vegetation indices, are considered the most used procedures for determining relationships/correlation (Candiago et al., 2015). The red and near-infrared (NIR) bands in the electromagnetic spectrum are used to calculate the frequently used VIs that is quite sensitive to the variations that occurred in the biophysical and chemical characteristics of the different vegetation (Cho et al., 2007). Therefore, researchers stated that both the Red and Blue spectral region observes low reflectance while the green area witnessed high reflectance in the case of the study carried out for vegetation (Bachmann et al., 2013). Thus, according to the variation that occurred in reflection due to the absorption of chlorophyll in the visible portion of the electromagnetic spectrum, different types of VIs react accordingly. To estimate the canopy height of crops and the biomass of the vegetation, utilization of vegetation indices (VIs) depending upon several multispectral (Geipel et al., 2016) or hyperspectral data (Aasen et al., 2015) is done by numerous researchers in their studies.

The Normalized Difference Vegetation Index (NDVI) is the most widely used index due to its simplicity and strong empirical correlation with vegetative productivity and leaf area index (Carlson & Ripley, 1997; Huete et al., 2002). Zheng et al. (2007) demonstrated that the red (Band 4) and near-infrared (NIR; Band 5) spectral bands serve as effective predictors of biomass. Similarly, Foody et al. (2003) reported strong correlations between biomass and vegetation indices such as the NDVI. Poudel et al. (2023) reported that NDVI was the most precise vegetation index for estimating and mapping aboveground biomass and carbon stocks in Nepal's Chure region. However, NDVI suffers from saturation in high biomass or dense canopy conditions, which leads to systematic underestimation of AGB in such environments (Myneni et al., 1995; Lu et al., 2016). Zhu and Liu (2015) demonstrated that seasonal variations, especially fall-season NDVI, provide stronger correlations with field-measured AGB than peak growing season values, mitigating saturation and yielding more reliable biomass estimates. To overcome NDVI limitations, indices such as the Enhanced Vegetation Index (EVI) have been developed and applied. EVI incorporates the blue band to correct for atmospheric and soil background influences, thereby improving sensitivity in dense forests (Huete et al., 2002). Zhao et al. (2016) emphasized that vegetation indices respond differently across forest types and biomass gradients, underscoring the need to select and combine indices appropriately for specific ecosystems.

2.3. Modeling Approaches: From Regression to Machine Learning

The estimation of aboveground biomass (AGB) using remote sensing data has undergone significant methodological evolution, reflecting both technological advancements and growing understanding of vegetation-spectra relationships. Early approaches predominantly employed linear regression techniques, valued for their computational efficiency and straightforward interpretation (Lu et al., 2016). These models typically established direct relationships between spectral predictors (e.g., NDVI, EVI, or individual bands) and AGB, performing adequately in homogeneous environments with uniform vegetation structure. However, their effectiveness diminishes markedly in heterogeneous landscapes where complex variations in vegetation density, species composition, and canopy architecture prevail (Foody et al., 2003).

The fundamental limitation of linear approaches lies in their inability to capture the nonlinear dynamics inherent in vegetation-spectra interactions. Polynomial regression emerged as an intermediate solution, with studies such as Zheng et al. (2007) demonstrating improved performance through quadratic NDVI terms in tropical forests. Nevertheless, these models introduced new limitations, including susceptibility to overfitting with higher-order terms and poor generalization across diverse ecosystems (Lu et al., 2016).

The recognition of these limitations catalyzed a paradigm shift toward machine learning (ML) approaches, enabled by advancing computational capabilities and increased data availability. Modern ML algorithms, including Random Forest (RF), Support Vector Regression (SVR), and XGBoost, offer distinct advantages through their capacity to model complex nonlinear relationships without restrictive distributional assumptions (Belgiu & Drăguţ, 2016). These models are appealing because they are non-parametric, can handle different types of predictor variables, are easy to implement, and generally produce low prediction errors (Powell et al., 2010). However, no single modeling approach is universally superior; the best choice depends on the study's objectives, such as minimizing prediction error, preserving variance, or maintaining covariance structure (Powell et al., 2010; Zhu & Liu 2015).

An emerging consensus from these investigations highlights a critical balance between algorithmic selection and data quality. Zhu and Liu (2015) seminal work demonstrated that temporal data richness exerts greater influence on model accuracy than algorithm choice itself, with multi-temporal datasets consistently outperforming single-date inputs across all tested methods. This insight underscores the dual importance of both methodological sophistication and robust data acquisition strategies in contemporary AGB estimation (Zhu et al., 2020).

2.4. Temporal and Multi-Seasonal Data Integration

Accurate estimation of aboveground biomass (AGB) is critical for carbon cycle modeling, forest management, and climate change mitigation (Goetz & Dubayah, 2011; Saatchi et al., 2011). Traditional remote sensing approaches relying on single-date or peak-growing season imagery often suffer from spectral saturation in high-biomass regions, leading to underestimation (Mutanga et al., 2004; Lu et al., 2016). To address this, recent studies emphasize integrating multi-seasonal and multi-temporal remote sensing data, which capture phenological variability and improve AGB prediction accuracy (Powell et al., 2010; Anees et al., 2024).

Data collected at different times captures different aspects of forest structure, which influences aboveground biomass (AGB). Peak growing seasons primarily represent canopy top characteristics. Dense canopies often cause reflectance saturation in optical sensors, limiting their sensitivity to high AGB levels (Dube & Mutanga, 2004). However, off-peak imagery (e.g., early spring or late autumn) can mitigate this issue by exposing underlying vegetation structure and reducing saturation effects (Musthafa & Singh, 2022). Consistent with these considerations, Li et al. (2020) found that in a subtropical forest of northern Hunan Province, China, time-series images from different seasons can affect AGB estimation, with autumn imagery (October) providing the most accurate estimates, whereas peak-season imagery (August) yielded poorer results.

Integrating environmental covariates such as topography and climate into biomass estimation models substantially increases their explanatory power by capturing physical and climatic controls on vegetation structure and productivity. Topographic variables—including elevation, slope, aspect, and derivatives like the Topographic Wetness Index (TWI)—shape local microclimate, soil moisture, and solar radiation, thereby affecting biomass distribution patterns (Hojo et al., 2023; Ma et al., 2025).For instance, elevation and aspect have been shown to correlate strongly with above-ground biomass (AGB) variation in temperate forests, with the highest biomass often observed in specific elevation or aspect ranges (Muhammad et al., 2024). These variables can act as proxies for biophysical and ecological process gradients affecting vegetation growth (Li et al., 2008).

The contribution of climatic variables—such as precipitation and temperature—is more context-dependent, varying with biome, spatial scale, and predictor temporal resolution. Several studies have demonstrated that mean annual temperature and precipitation significantly influence biomass distribution by driving net primary productivity and eco-physiological processes (Chave et al., 2014; Zhang et al., 2019). Integrating climatic and soil factors into biomass modeling systems for varied forest types has been shown to enhance predictive accuracy, especially when combined with traditional biotic measurements (Saatchi et al., 2011). Zhao et al. (2016) demonstrated that stratifying AGB estimation models by vegetation type and topography can effectively mitigate Landsat TM reflectance saturation, reducing RMSE from 29.3 to 24.5 Mg/ha and improving estimation accuracy.

While multi-temporal and multi-seasonal remote sensing approaches have been explored, many applications remain constrained by limited seasonal coverage, single-image-per-year strategies, or incomplete integration with topographic variables. This study advances AGB estimation by leveraging stacked NDVI, EVI, and NBR time series across multiple years and seasons, combined with topographic predictors.

3. Methodology

3.1. Study Area

The research was conducted within the Kankali Community Forest (CF), located in Khaireni Municipality, Chitwan District, Bagmati Province, Nepal (27.65°N, 84.57°E). This site forms part of a long-term ecological monitoring initiative under the "Community-based Forestry in the Nepal Himalaya" (ComForM) project, coordinated by the Institute of Forestry, Tribhuvan University. As one of the few community forests in Nepal with repeated long-term measurements, Kankali CF represents a valuable data source within the national Community Forest Program. Geographically, the forest lies in the tropical lowlands (Terai region) and spans an elevation gradient from approximately 220 to 580 meters above sea level, encompassing a total area of 749.13 hectares. The dominant forest type is *Shorea robusta* (Sal) forest, interspersed with several light-demanding co-dominant species, including *Lagerstroemia parviflora*, *Dalbergia sissoo*, and *Semecarpus anacardium* (Baral & Vacik, 2018).

Historically, Kankali Community Forest in Chitwan, Nepal, suffered severe depletion due to overharvesting, land conversion, and uncontrolled extraction, resulting in extensive forest degradation and loss of vegetation cover (Grassroots Global, 2017). In response, community-based management was introduced in 1995, shifting the focus to strict protection measures, regulated harvesting based on operational plans, and active replantation dominated by native Sal (*Shorea robusta*) species. Since then, the forest has recovered to a dense, regenerating pole-stage stand. Current harvesting focuses on a selective system that removes dead, diseased, and deformed trees to maintain a stable growing stock, ensuring sustainable timber supply while promoting healthy forest regeneration (Baral et al., 2025).

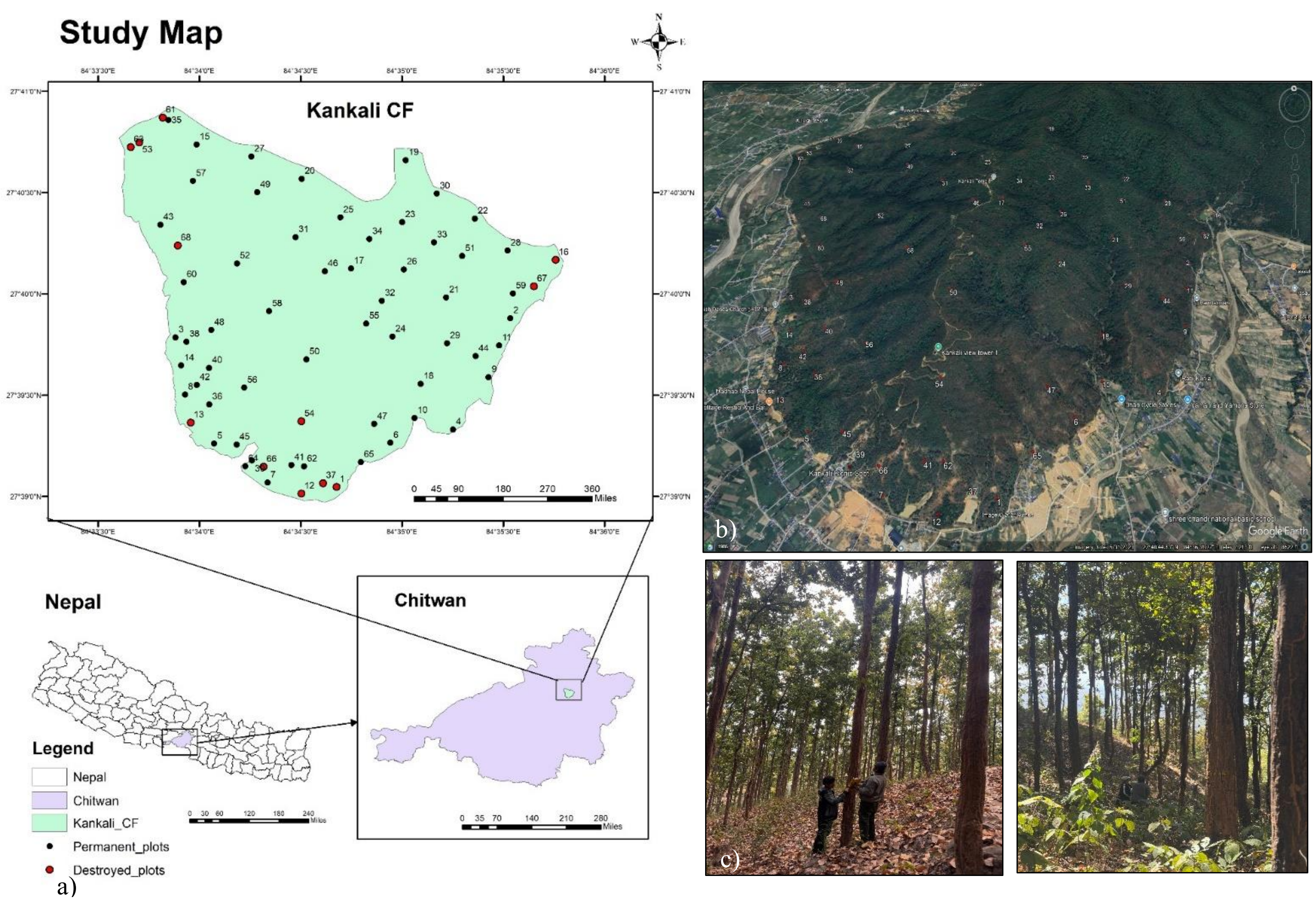

Figure 1: a) boundary map of Kankali community forest, b) plots position in Kankali Cf, c) trees within the plot

3.2. Research Design

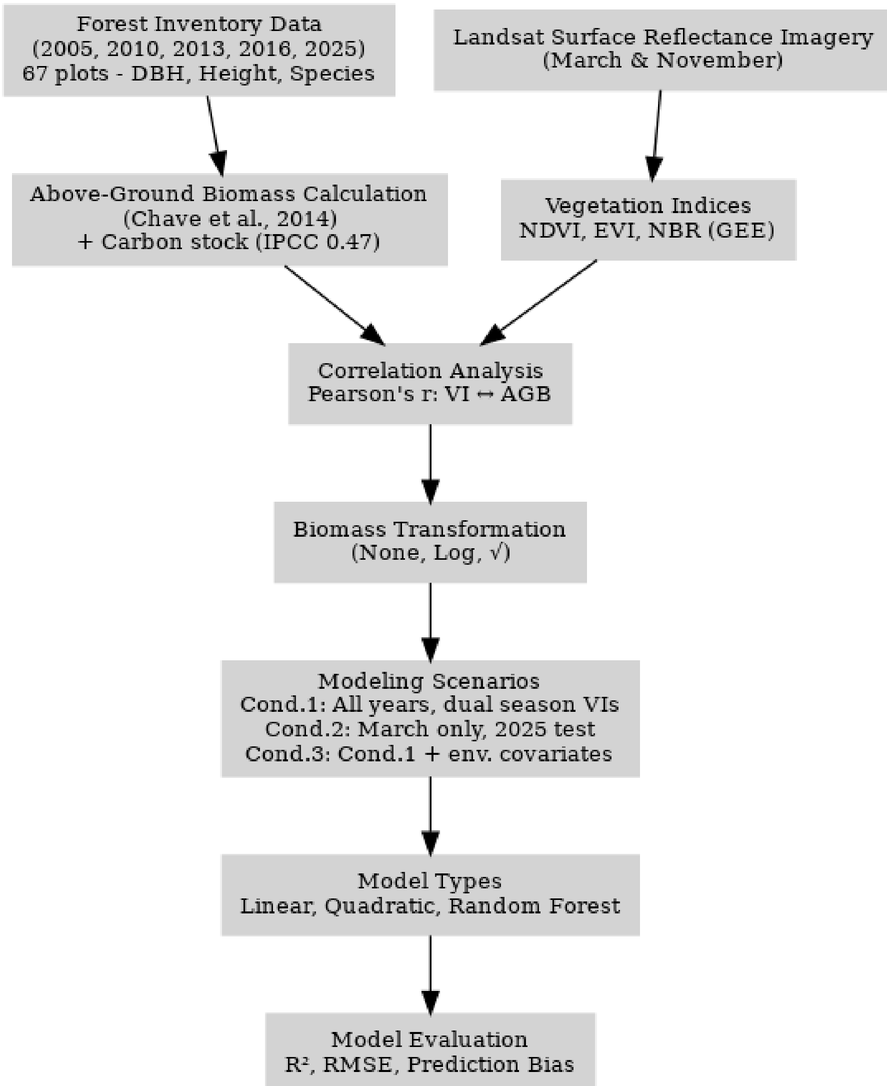

Figure 2: Methodological Framework of the research process

3.3. Data Collection

3.3.1. Field Based Observation

This study utilized forest inventory data collected through the ComForM project during the years 2005, 2010, 2013, and 2016. The initial sampling followed a restricted random design based on the "coffee-house" principle (Müller, 2001), as described by Puri et al. (2012). In this approach, the first plot was selected randomly, and subsequent plots were positioned to maximize the minimum distance from existing plots, thereby promoting spatial dispersion across the study area. A total of 68 permanent sample plots were originally established in Kankali CF (Figure 1b). For the purposes of this study, 67 plots were identified, and field inventory was conducted from February-March 2025. One plot (Plot 16) was excluded as it fell within a restricted military zone (army barracks), however including the destroyed plots excluded in previous study due to loss from land-use change and infrastructure development (Baral et al., 2025).

Each permanent plot measured 20 m × 25 m and included nested subplot to accommodate the measurement of trees across different diameter classes. Trees with a diameter at breast height (DBH) greater than 10 cm were measured in the full 20 × 25 m plot. Meanwhile, smaller trees with DBH between 4 cm and 9.9 cm were measured within a nested 10 × 15 m subplot. DBH was measured at 1.3 m above ground using diameter tape. Species identification, tree height and coordinates were recorded for each tree. Permanent plots were located using GPS and confirmed in the field by the presence of concrete pillars at the corners and paints on trees.

Tree height (H, m) was estimated from DBH (cm) using the log-linear model:

$$H=9.7436\times\ln(DBH)-12.916$$

This equation was applied to maintain consistency with previous measurements from the same permanent plots. The log-linear height–diameter model form ($H = a+b\ln(DBH)$) is widely used in forestry (Curtis, 1967) for reliable height estimation when direct measurements are impractical.

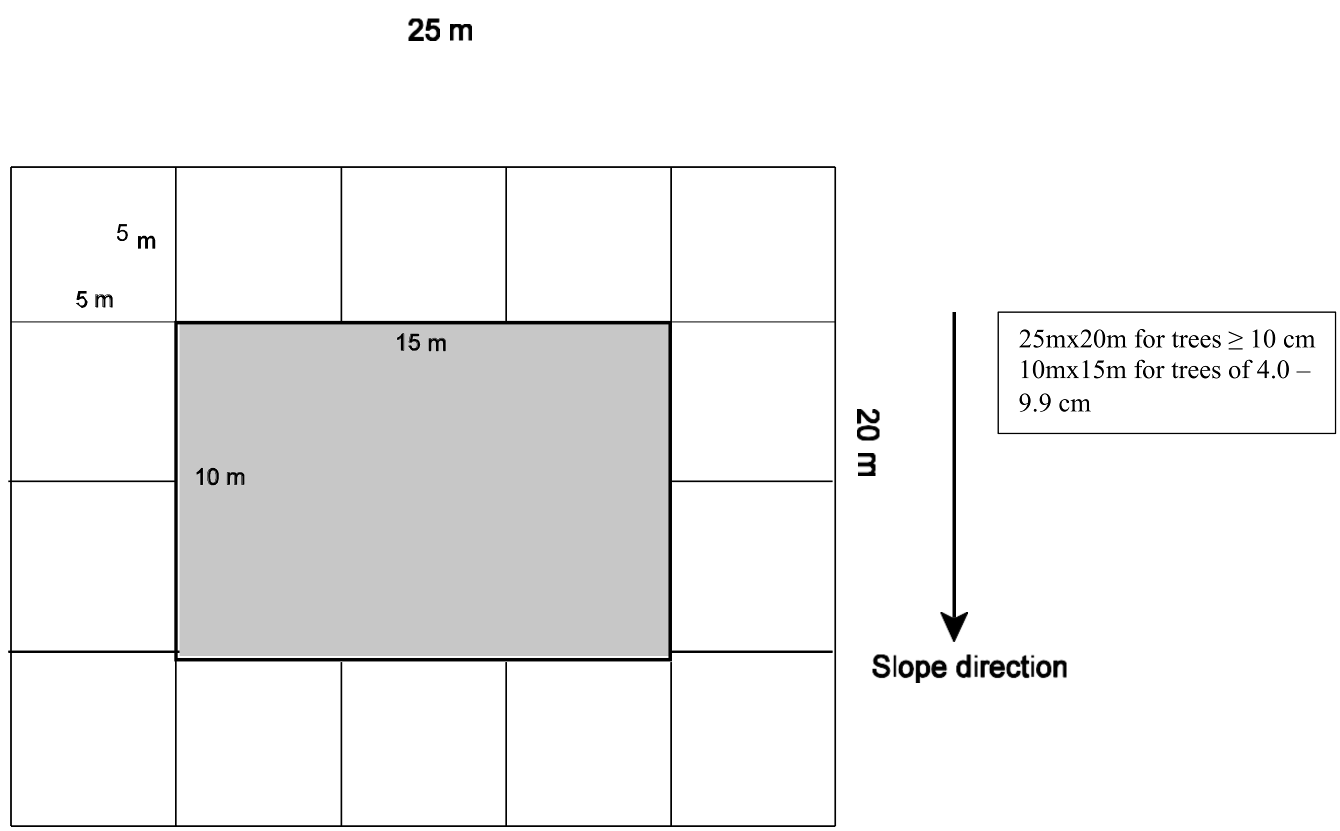

Figure 3:Plot structure used in ComForm long term study for trees above 4cm dbh

3.3.2. Satellite Imagery datasets

Satellite imagery was sourced from Google Earth Engine (GEE), which hosts USGS Landsat Collection 2, Tier 1 surface reflectance products. Landsat 5 Thematic Mapper (TM) images were used for the years 2005 and 2010, while Landsat 8 Operational Land Imager/Thermal Infrared Sensor (OLI/TIRS) images were used for 2013, 2016, and 2025. Image acquisition dates were initially selected by visually inspecting scenes on USGS Earth Explorer to ensure minimal cloud contamination (less than 10% cloud cover). The corresponding scenes were then retrieved in GEE by their unique Landsat Scene IDs. Information on acquisition dates and scene IDs is provided in Appendix 1. The spectral bands used for vegetation index computations were Red, Blue, Near-Infrared (NIR), and Shortwave Infrared (SWIR), as detailed below:

Table 1: Bands' information for image datasets

Platform	Bands Used	Wavelength (µm)	Spatial Resolution (m)
Landsat 5 TM	Band 1 (Blue), Band 3 (Red), Band 4 (NIR), Band 5 (SWIR)	0.45–0.52, 0.63–0.69, 0.76–0.90, 1.55–1.75	30
Landsat 8 OLI	Band 2 (Blue), Band 4 (Red), Band 5 (NIR), Band 6 (SWIR)	0.45–0.51, , 0.64–0.67, 0.85–0.88, 1.57–1.65	30

3.3.3. Environmental data:

Environmental data for temperature, precipitation, and potential evapotranspiration were obtained from the CRU CY dataset, which provides country-level monthly, seasonal, and annual climate averages derived from the CRU TS (Climatic Research Unit gridded Time Series) dataset. CRU TS is a globally recognized climate dataset based on the interpolation of monthly climate anomalies from extensive weather station networks, available at a 0.5° × 0.5° spatial resolution (Harris et al., 2020). The dataset spans from 1901 to 2018 and is regularly updated. For this study, data specific to Nepal were extracted to represent the environmental conditions of the study area.

3.4. Data Computation

3.4.1. Above-ground biomass calculation and carbon estimation

This study focused on the AGB estimates derived from the permanent sample plots for the years 2005, 2010, 2013, 2016 and 2025. With the data of individual trees collected in the field within a sample plot, AGB was calculated using the allometric equation described by Chave et al. (2014).

$$AGB=0.0673*(\rho.\ D\text{^}2.H)\ ^{\text{^}0.976}$$

Where, AGB = above-ground biomass (kg), ρ = wood specific gravity (gm/cm3), D = tree diameter at breast height (cm), and H = tree height (m).

The wood specific density was derived from various literature reviews. Species with their default specific values (ρ) given by Khanna & Chaturvedi (1982); FRTC (2022) were used to calculate tree level biomass. In the absence of specific values, general values (ρ = 0.674) (Pandit et al., 2018) were used (Appendix 2).

Using the IPCC (2006) default carbon fraction of 0.47 biomass stock densities were converted to carbon stock.

Carbon stock= AGTB*0.47

3.4.2. Image processing:

For consistency and temporal coverage, Landsat surface reflectance (SR) products were used. Two representative phenological stages were analyzed for each study year: March (dry season) and November (post-monsoon season). All image processing was conducted in Google Earth Engine (GEE). Cloud and cloud-shadow masking were applied to all Landsat scenes using the QA_PIXEL bitmask provided in Landsat Collection 2, Tier 1 surface reflectance products (bits 3 and 5 correspond to cloud shadow and cloud). After applying this quality mask, images were clipped to the Kankali CF study boundary.

3.4.3. Plot Buffering

Field plot centroids (n = 68) were geolocated and imported into GEE as a Feature Collection. Around each centroid, a 12.5-meter radius buffer was applied to better represent the spatial footprint of the original 20 × 25 m plots, while accounting for geolocation uncertainty and mixed-pixel effects.

3.4.4. Spatial Data Collection and Analysis

There are over 150 different VIs available, but only three indices—NDVI, EVI, and NBR—were selected for this study based on their effectiveness in previous studies in analyzing and predicting AGB. These indices were calculated using spectral bands from the Landsat imagery, specifically the Red, Near-Infrared (NIR), Blue, and Shortwave Infrared (SWIR-1) bands.

1. Normalized Difference Vegetation Index (NDVI):

NDVI=(NIR-Red)/(NIR+Red)
(Gitelson & Merzlyak, 1997)

2. Enhanced Vegetation Index (EVI):

$$EVI = G \times \frac{(NIR - Red)}{NIR + C1 \times Red - C2 \times Blue + L}$$

(Huete et al., 2002)

(where G, C1, C2 and L are coefficients: typically, G=2.5, C1=6, C2=7.5, and L=1)

3. Normalized Burn Ratio (NBR):

$$NBR = (NIR - SWIR)/(NIR + SWIR)$$

Key and Benson (1999)

3.5. Statistical analysis:

Statistical analyses and biomass modeling were conducted using Microsoft Excel and R Studio. Pearson's correlation coefficient was first calculated to examine relationships between vegetation indices (VIs) and above-ground biomass (AGB). To address potential heteroscedasticity in the response variable, biomass data were analyzed using three transformations: untransformed, logarithmic, and square root. Model performance for each transformation was evaluated using the coefficient of determination (R^2) and root mean square error (RMSE) to identify the most suitable transformation for subsequent analyses.

To address the study objectives and data availability, the analysis was organized into three distinct modeling scenarios. Scenario 1 included all years except 2025 (2005, 2010, 2013, and 2016) and used all six vegetation indices (NDVI, EVI, and NBR from both March and November) as predictors. This approach was designed to evaluate whether incorporating dual-seasonal information could improve the prediction of aboveground biomass (AGB) compared to single-season inputs. Scenario 2 assessed single-season performance and temporal transferability through three configurations: (a) November-only (NDVI_Nov, EVI_Nov, NBR_Nov) from 2005–2016, (b) March-only (NDVI_March, EVI_March, NBR_March) from the same years — both with 80 %/20 % random splits for direct seasonal comparison — and (c) March-only with a temporal transferability test, training on 2005–2016 March data and testing on independent 2025 march data. Scenario 3 extended the predictors used in Scenario 1 by adding plot elevation and coarse-resolution monthly climate variables (temperature, precipitation, and potential evapotranspiration), to test whether these ancillary variables could improve model performance. For Scenarios 1 and 3, the data were randomly split into 80% training and 20% testing subsets.

In this study, two parametric regression approaches: simple linear regression and quadratic regression, were employed alongside a non-parametric machine learning approach. Simple linear regression, one of the most widely used empirical modeling techniques, applies ordinary least squares to estimate parameters of a linear relationship between a single predictor variable and a field-measured biophysical parameter (du Plessis, 1999; Drake et al., 2003). However, as noted in previous studies, this approach may be limited when the relationship is inherently non-linear or when a single predictor variable cannot adequately explain the variation in the dependent variable. To address potential non-linearity, quadratic regression was applied by including squared terms for the predictor variables, enabling the model to capture curvilinear relationships between spectral indices and AGB that would not be represented in a purely linear model (Poudel et al., 2023). Non-parametric approaches such as RF are particularly well-suited for capturing complex, non-linear relationships between biophysical variables and remotely sensed data, and have been widely applied in ecological remote sensing to reduce overfitting risks while maintaining high predictive accuracy (Powell et al., 2010; Avitabile et al., 2012; Main-Knorn et al., 2013).

In this study, all three modeling methods were implemented for both scenarios 1 and 2, while only the linear regression model was fitted for condition 3.

3.6. Accuracy assessment

Model performance was assessed on both training and testing datasets using metrics: (i) root mean square error (RMSE), the measure of prediction error, where smaller values indicate better fit; (ii) the coefficient of determination (R^2), indicates how well the observed AGB is predicted by the model by representing the proportion of the total variation in AGB explained by the predictors. In general, a higher R^2 value reflects stronger model performance (Li et al., 2020).

Root Mean Squared Error (RMSE)

$$\boldsymbol{RMSE} = \sqrt{\frac{\sum_{i=0}^{n} (Yi - \hat{Y}\imath)^2}{n - p}}$$

Where Yi and $\hat{Y}\imath$ are observed and predicted AGB value of the ith plot respectively, and n is the total number of plots.

4: Results

4.1. Aboveground Biomass Trends Across Study Years

Field inventory data revealed a consistent increase in aboveground biomass (AGB) over the study period in Kankali Community Forest. The average biomass per hectare was calculated for each inventory year and showed a steady upward trend: 105.52 t/ha in 2005, 137.58 t/ha in 2010, 163.10 t/ha in 2013, 189.09 t/ha in 2016, and reached 210.71 t/ha in 2025.

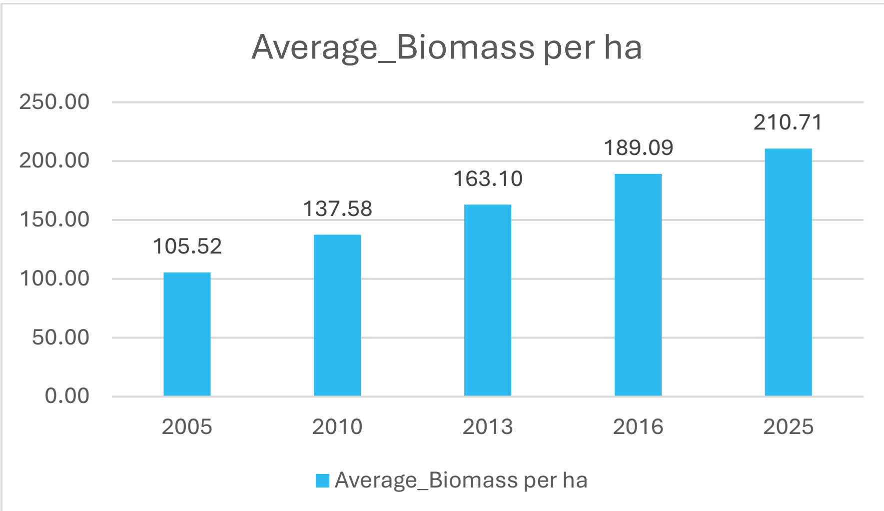

Figure 4: Average biomass per ha(ton/ha) across all years

4.2. Biomass Transformation and Selection

Variable transformations are essential in biomass modeling to address common issues such as heteroscedasticity and non-normal residuals that can bias regression estimates (Porté & Bartelink, 2002; Sileshi, 2014). The main objective of applying these transformations was to satisfy linear regression assumptions, ensuring reliable and unbiased parameter estimation. Before modeling, three response variable transformations were evaluated to determine the most suitable format for biomass data: no transformation (Biomass_none), square root transformation (Biomass_sqrt), and logarithmic transformation (Biomass_log). Model evaluation was based on RMSE and R^2 metrics using linear regression models with six vegetation indices as predictors (NDVI, EVI, and NBR from both March and November). The results are shown in Table 2.

Table 2: Accuracy Assessment of biomass transformation

Transformation	**RMSE**	**R^2**
Biomass_none	84.6	0.579
Biomass_sqrt	**82.9**	**0.694**
Biomass_log	94.3	0.557

The square root transformation (Biomass_sqrt) produced the lowest RMSE (82.9) and the highest coefficient of determination ($R^2 = 0.694$), indicating better predictive performance and better normalization of residual variance. Therefore, all subsequent models in this study used Biomass_sqrt as the response variable.

4.3. Correlation Between Vegetation Indices and Biomass

Pearson correlation coefficients were computed between field-measured above ground biomass and each vegetation indices: Normalized Difference Vegetation Index (NDVI), Enhanced Vegetation Index (EVI), and Normalized Burn Ratio (NBR), across multiple years and both seasons (Appendix 3 and 4). Table 3 presents a subset of the correlation results derived from field data and satellite imagery. The key findings are as follows:

Table 3:Correlation coefficient (r) between each Vegetation Indices across multiple years and both seasons and biomass

Year	**NDVI_March**	**NDVI_Nov**	**EVI_March**	**EVI_Nov**	**NBR_March**	**NBR_Nov**
2005	0.360	0.471	0.344	0.672	0.496	0.613
2010	0.483	0.537	0.535	0.701	0.404	0.661
2013	0.493	0.500	0.474	**0.769**	0.497	0.605
2016	**0.622**	0.517	0.555	0.676	0.378	0.730
2025	0.387	—	0.393	—	0.431	—

Across all years, vegetation indices derived from post-monsoon (November) imagery generally exhibited stronger correlations with AGB than those from the dry season (March). In particular, EVI_Nov consistently showed the strongest correlations, with values as high as $r = 0.769$ in 2013 and $r = 0.701$ in 2010.

NDVI_Nov typically outperformed NDVI_March, $r = 0.537$ in 2010 vs. $r = 0.483$ in March, except in 2016, where NDVI_March showed a stronger correlation ($r = 0.622$). Similarly, NBR_Nov exhibited higher correlations with AGB ($r = 0.730$ in 2016) compared to NBR_March ($r = 0.378$ in 2016).

While vegetation indices from March were still moderately correlated with AGB, they generally yielded lower correlation values. The correlations between AGB and the vegetation indices (NDVI, EVI, and NBR) were statistically significant across all study years and seasons, as all p-values were below the 0.05 significance threshold corresponding to the 95% confidence level (Appendix 4).

4.4. Biomass Modeling Results

Three modeling scenarios were tested to assess predictive accuracy and understand the influence of seasonality and auxiliary variables.

4.4.1 Scenario 1: Using multi-seasonal (March and November) Vegetation Indices

This scenario used both March and November values of NDVI, EVI, and NBR as predictors across four years (2005, 2010, 2013, and 2016).

The Random Forest model achieved the highest predictive performance on both training ($R^2 = 0.94$) and test ($R^2 = 0.62$) datasets, indicating strong generalization capability. In contrast, the linear and quadratic models performed similarly on the test data, with R^2 values of 0.58, with RMSEs of 84.62 and 85.61, respectively. These results indicate that the RF model was better able to capture complex, non-linear interactions among predictors.

The linear model equation for this scenario was:

$$y = -242.604 + 76.182 \times NDVI\_March + 78.559 \times NDVI\_Nov + 148.651 \times EVI\_March + 367.268 \times EVI\_Nov - 14.45 \times NBR\_March + 205.081 \times NBR\_Nov$$

Among these vegetation indices, NDVI_Nov, EVI_Nov, and NBR_Nov had statistically significant positive effects on the response variable ($p < 0.05$), with relatively small standard errors indicating precise estimates (see Appendix 2 for detailed parameter estimates and standard errors). NDVI_March and EVI_March also showed positive effects but with marginal significance ($p \approx 0.05$). While the coefficient for NBR_March was negative (−14.45), it did not reach statistical significance ($p = 0.161$), indicating limited predictive contribution in the presence of other variables (Appendix 5A1).

Training Result

Testing Result

Linear Regression

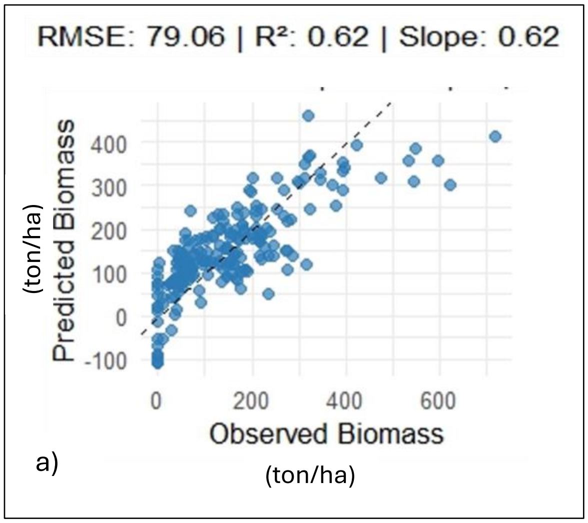

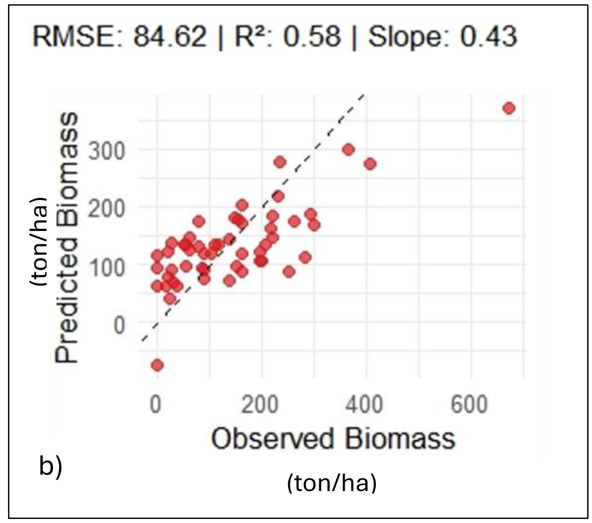

Quadratic Regression

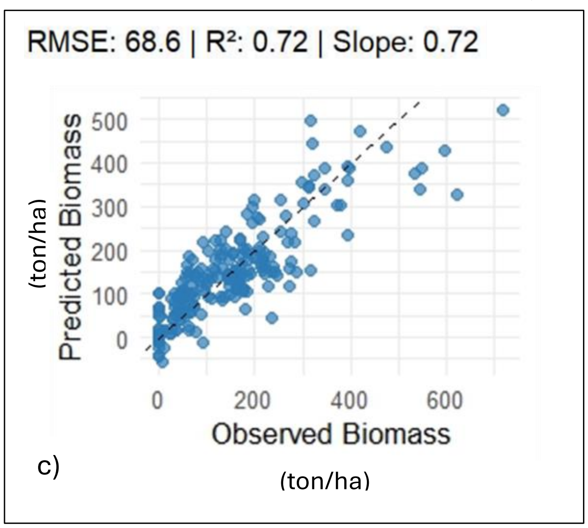

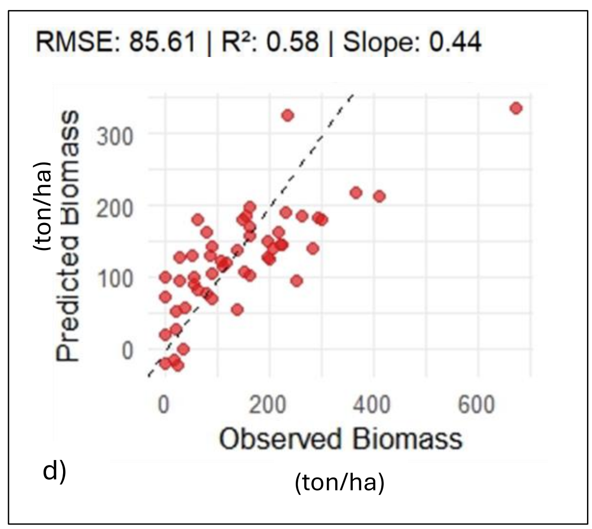

Random Forest

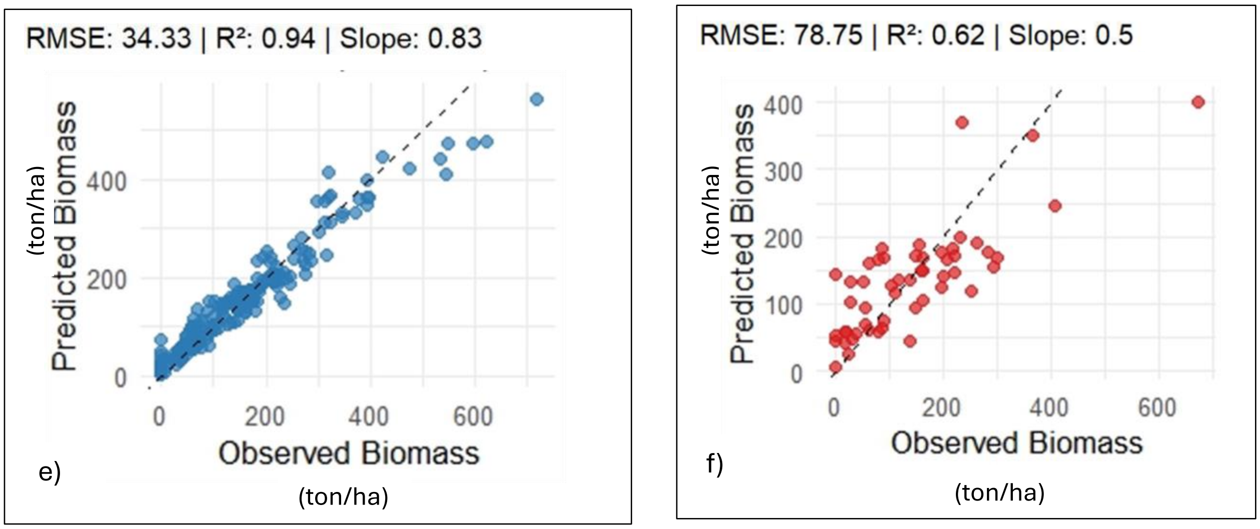

Figure 5: Observed AGB vs. predicted AGB by linear regression for (a) training and (b) testing, quadratic regression for (c) training and (d) testing, random forest for (e) training and (f) testing- with multi-seasonal VIs.

4.4.2 Scenario 2: Single Season Vegetation index

4.4.2.1. November VIs-Only

This scenario used NDVI_Nov, EVI_Nov, and NBR_Nov as predictors across four years (2005, 2010, 2013, and 2016). The Random Forest model achieved the highest predictive accuracy on the training dataset (R2=0.92, RMSE = 39.364), indicating strong model fit. However, on the test dataset, Random Forest performance decreased (R2=0.66, RMSE = 79.492), and the differences from the linear (R2=0.66, RMSE = 84.246) and quadratic (R2=0.69, RMSE = 80.897) models were relatively small.

The linear model equation for this scenario was:

y = -6.6685 + 9.9*NDVI_Nov + 15.2865*EVI_Nov + 5.6357*NBR_Nov

In the linear model, all three vegetation indices were statistically significant ($p<0.001$), with relatively small standard errors (Appendix 5A2). In the quadratic model, NDVI_Nov exhibited a significant nonlinear pattern, with a negative linear term and a positive squared term, indicating curvature in the relationship. EVI_Nov showed only borderline evidence of curvature ($p \approx 0.069$) and NBR_Nov contributed no significant nonlinear effect.

In comparison to the combined March–November scenario, the November-only models showed slightly higher R^2 and lower RMSE for both the linear model (R^2: 0.666 vs. 0.580; RMSE: 84.246 vs. 84.620) and the quadratic model (R^2: 0.694 vs. 0.580; RMSE: 80.897 vs. 85.610). For Random Forest, performance was similar between scenarios, with negligible differences in opposite directions.

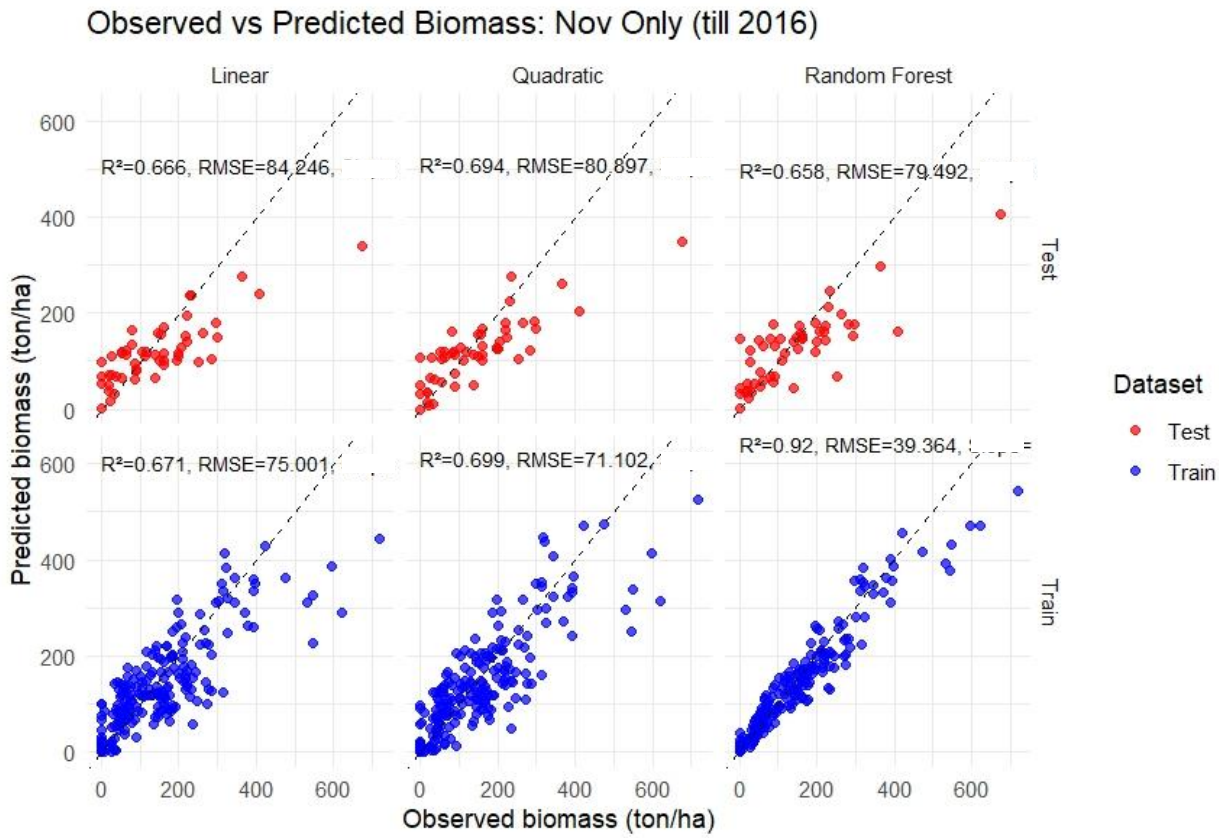

Figure 6: Observed AGB vs. predicted AGB for testing and training by linear regression, quadratic regression and random forest- with November VIs only.

4.4.2.2. March VIs only-

This scenario used NDVI_March, EVI_March, and NBR_March as predictors for the years 2005, 2010, 2013, and 2016. The Random Forest model achieved the highest predictive accuracy on the training dataset ($R^2 = 0.851$, RMSE = 64.06), substantially outperforming the parametric models. However, in the test dataset, Random Forest performance declined ($R^2 = 0.209$, RMSE = 112.01), and the differences from the linear model ($R^2 = 0.330$, RMSE = 104.01) were relatively modest. The quadratic model showed the lowest predictive performance in this scenario ($R^2 = 0.075$, RMSE = 121.62), indicating limited benefit from including nonlinear terms.

Linear Model:

y = 6.4915 + 4.8522*NDVI_March + 7.7695*EVI_March + 12.2235*NBR_March

In the linear model, only NBR_March was statistically significant ($p < 0.001$), while NDVI_March ($p = 0.123$) and EVI_March ($p = 0.163$) were not. The quadratic model included significant positive effects for NDVI_March and NBR_March and a significant negative squared term for NDVI_March, but its overall predictive capability was reduced compared with the linear model (full coefficients and standard errors in Appendix 5A3).

Compared with the combined March–November scenario, the March-only models generally demonstrated weaker predictive performance. Both the linear (R^2: 0.330 vs. 0.580; RMSE: 104.017 vs. 84.62) and quadratic (R^2: 0.075 vs. 0.580; RMSE: 121.804 vs. 85.61) models yielded lower accuracy. For Random Forest, performance was also reduced in the March-only case (R^2: 0.209 vs. 0.620; RMSE: 112.199 vs. 78.75). Relative to the November-only scenario, March-only results were similarly less accurate across all three modeling approaches, underscoring the stronger predictive value of the November dataset in this study.

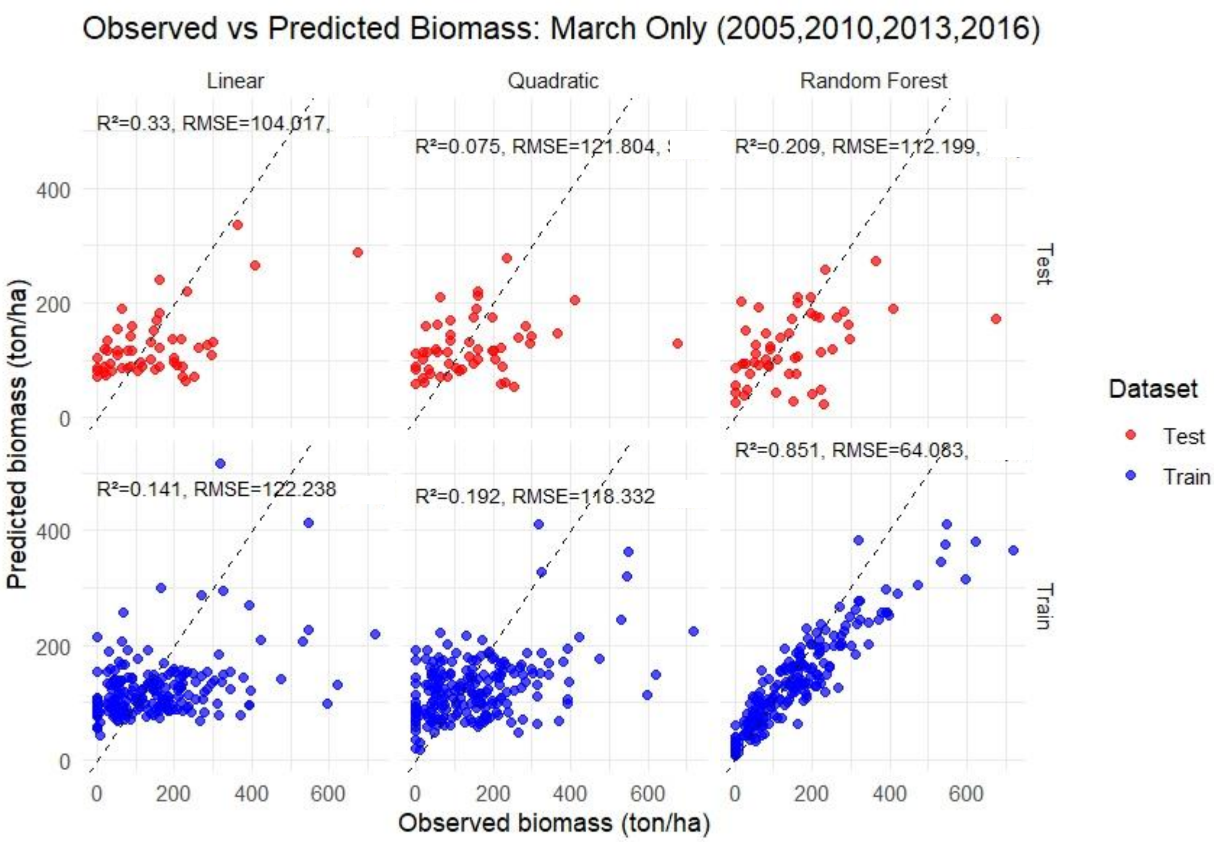

Figure 7: Observed AGB vs. predicted AGB for testing and training by linear regression, quadratic regression and random forest- with March VIs only.

4.4.2.3. March Indices Only (with 2025 as Test Year)

This model assessed performance using only March indices, with 2025 reserved exclusively for testing.

Results indicated a notable drop in model accuracy when trained solely on March data and tested on 2025. Despite good training performance (R^2 = 0.86), the Random Forest model's test accuracy dropped significantly (R^2 = 0.2), indicating poor generalizability to new data when using March indices alone. The Random Forest model achieved an RMSE of 153.67 on test data, while the linear and quadratic models on test data produced R^2 values of 0.19 and 0.21, respectively, with RMSEs exceeding 125 (full coefficients and standard errors in Appendix 5A4).

Training Result

Testing Result

Linear Regression

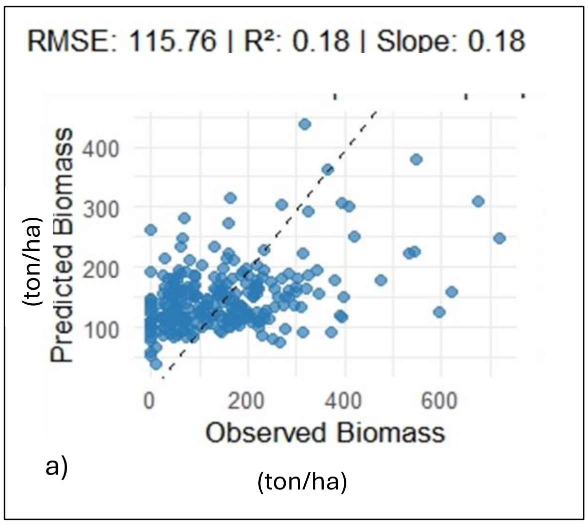

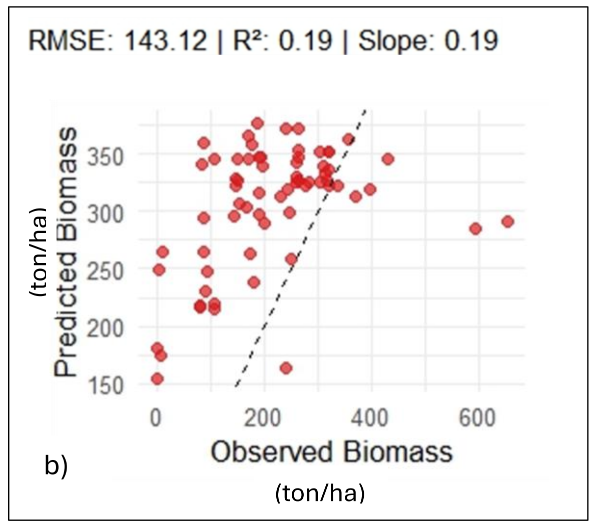

Quadratic Regression

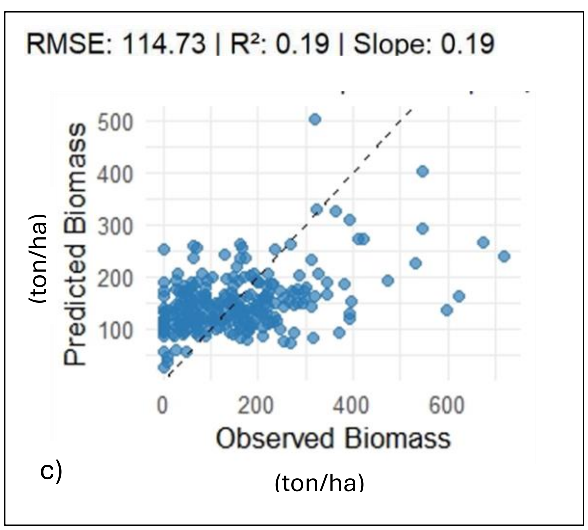

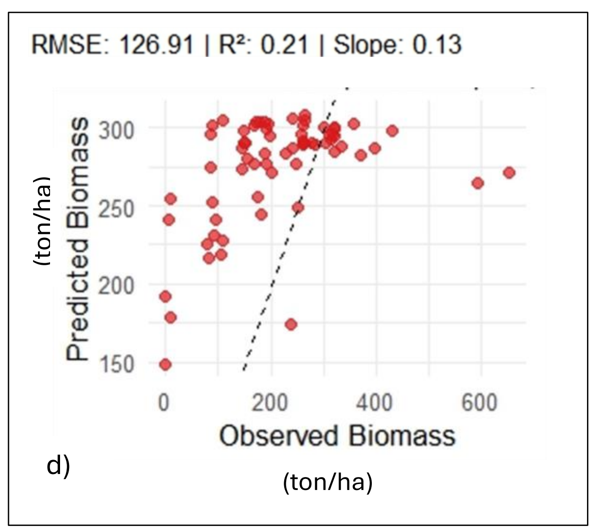

Random Forest

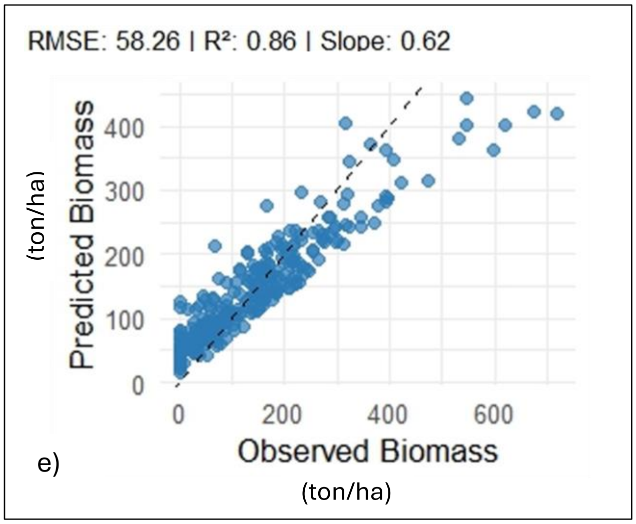

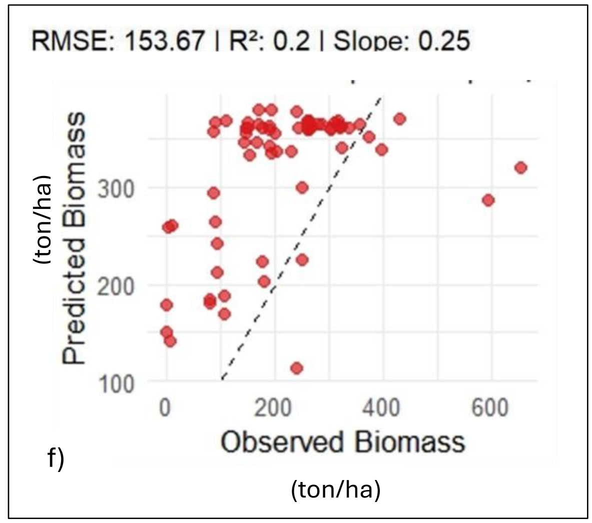

Figure 8: Observed AGB vs. predicted AGB by linear regression for (a) training and (b) testing, quadratic regression for (c) training and (d) testing, random forest for (e) training and (f) testing- with March VIs only with 2025 data.

4.4.3 Scenario 3: Inclusion of Weather and Elevation Variables

To explore whether incorporating elevation and weather variables would enhance model accuracy, a linear model was developed using vegetation indices (March and November), elevation, and monthly temperature, precipitation, and potential evapotranspiration data. This model was trained using all years except 2025 and tested on the remaining subset.

The model yielded an RMSE of 85.93 and R^2 of 0.57 on the test data, nearly identical to the linear model in Scenario 1. The inclusion of elevation and weather variables did not significantly improve model accuracy compared to the multi-seasonal Vegetation Indices model in Scenario 1.

Training Result

Testing Result

Linear Regression

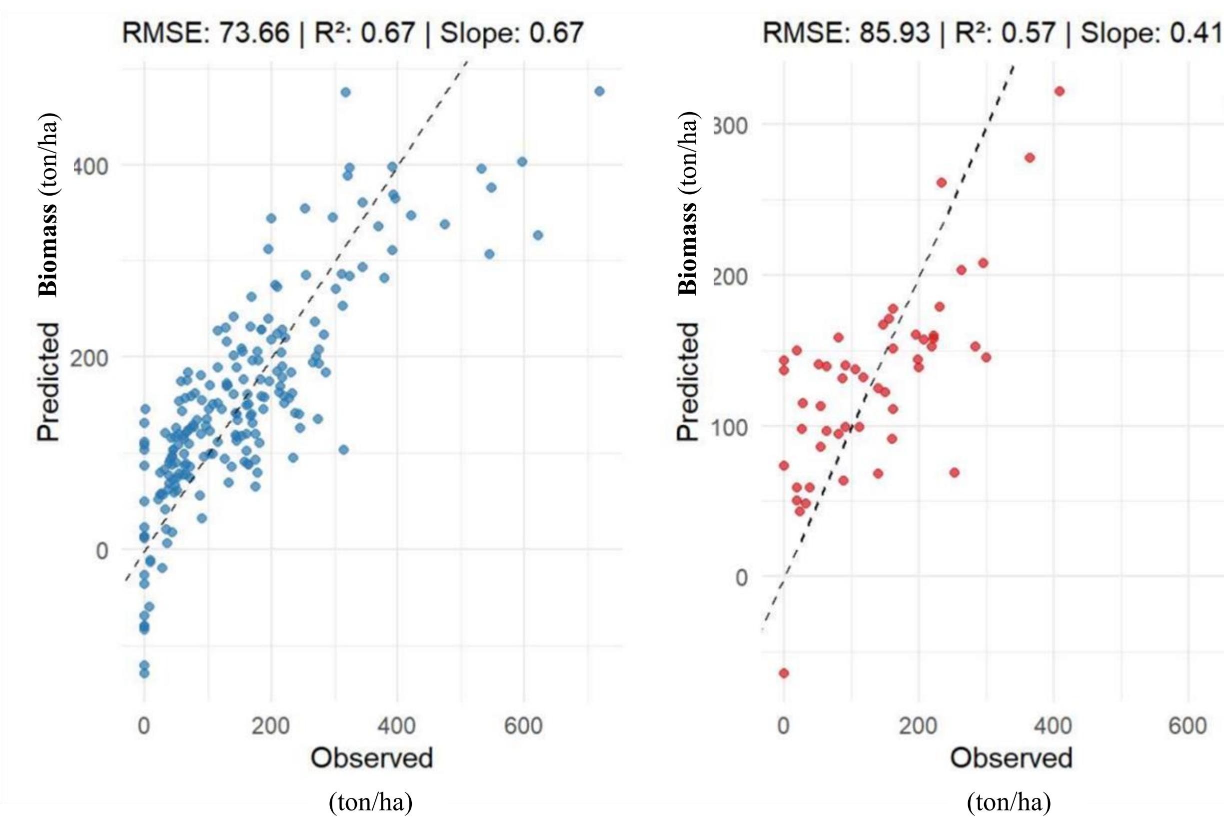

Figure 9: Observed AGB vs. predicted AGB by linear regression for training and testing, - with elevation and weather data.

4.5. Residual Analysis

Residuals from all three models were evaluated across all three scenarios.

For Scenario 1 (March + November VIs), residuals were approximately symmetric (skewness–0.06 to 0.03) with SDs 2.82–3.14. Linear and Quadratic residuals were normally distributed ($p > 0.5$), while RF showed slight non-normality ($p = 0.0013$). Residual SDs across fitted-value bins were consistent, indicating homoscedasticity.

In Scenario 2 (March VIs-only) and (November VIs-only), residuals were symmetric for November VIs (skewness –0.34 to –0.09) with SDs 3.01–5.23. For March VIs, residuals were roughly symmetric (skewness –0.13 to –0.09) with SDs 5.08–5.23. Linear and Quadratic residuals were normally distributed ($p > 0.4$), while RF showed minor non-normality. For, March VIs-only scenario testing 2025 data, residuals were positively skewed (~1.17–1.21) with higher SDs (≈115–118). Normality tests were significant ($p < 0.001$), and residual variability was larger in mid-range fitted values, reflecting challenges in temporal transferability. Scenario 3 showed moderate residual patterns, with no major violations detected.

Overall, residuals support good model performance for within 2005-2016 predictions, particularly with multi-seasonal predictors, while temporal transferability introduces higher variability and skewness.

5. Discussion

5.1. Interpretation of Field-Based Biomass Estimates:

The two decades of monitoring in Kankali Community Forest (CF) show a marked and consistent increase in aboveground biomass (AGB), reflecting both ecological recovery and the long-term influence of community-based forest management. This observed trajectory is best understood considering the forest's historical context and current structural characteristics. Kankali CF was extensively degraded in the early 1990s due to massive encroachment, illegal timber exploitation, and political instability, resulting in extensive canopy loss and low stocking densities (Grassroots Global, 2017). The handover to the local community in 1995 under Nepal's Community Forestry Program marked the beginning of a sustained recovery, facilitated by regulated harvesting, active protection, and enrichment planting in open patches (Grassroots Global, 2017). Kankali CF is dominated by *Shorea robusta*, which accounts for approximately 90% of the basal area (Grassroots Global, 2017), supplemented by a mix of light-demanding co-dominants such as *Lagerstroemia parviflora*, *Dalbergia sissoo*, and *Semecarpus anacardium* (Baral & Vacik, 2018). Because of synchronous regeneration following the disturbance in the early 1990s, the stand structure is reasonably uniform and nearly even in age. Baral et al. (2025) found that the selected harvesting system led to a significant increase in basal area from 13.4 to 23.1 m²/ha during an 18-year period. This trend is consistent with their findings. Their study noted that removal rates consistently remained below the forest's overall increment rate, allowing the stand to accumulate basal area, indicating a parallel rise in forest biomass under controlled extraction regimes.

According to the IPCC, the AGB range in Asia's tropical forests is 67.7 to 184.6 t/ha (Rozendaal et al., 2022). Kankali Community Forest has higher AGB than the IPCC-reported range, which can be attributed to its long-term protection under community management and the presence of mature, high-biomass species such as *Shorea robusta*. The findings are consistent with larger evidence that well-managed tropical secondary forests can serve as significant carbon sinks for decades after intensive usage ends (Pan et al., 2013). Baral et al. (2009) discovered that mature Sal forests in Nepal had the highest aboveground biomass compared to other forest types. Carbon stock (CS) and biomass in forests vary depending on species, forest type, age, canopy cover, stand structure, and altitude (Karki et al., 2016; Dar et al., 2017).

5.2. Relationship of Vegetation Indices and Seasonal Variation with Above-Ground Biomass

The correlation analysis between Landsat-derived vegetation indices (NDVI, EVI, NBR) and field-measured above-ground biomass (AGB) in Kankali Community Forest revealed positive relationships for both March (dry-season) and November (post-monsoon) imagery, with November showing consistently stronger and more significant correlations. This seasonal contrast aligns with well-established evidence that vegetation phenology and canopy condition markedly influence spectral–biomass relationships in forest ecosystems.

After the monsoon rains, increased leaf area index (LAI), canopy density, and chlorophyll concentration, enhance absorption in the red wavelengths and increase near-infrared (NIR) reflectance due to healthy internal leaf structure (Lu et al., 2016). Such conditions amplify the red–NIR contrast captured by sensors like Landsat, thereby strengthening the sensitivity of vegetation indices to biomass variation (Myneni et al., 1995; Carlson & Ripley, 1997). In contrast, March imagery typically represents a dry season with reduced canopy cover and increased leaf senescence or stress, diminishing the spectral signal related to biomass. This seasonal decline in canopy greenness reduces the dynamic range of VIs and increasing background noise from litter and bare branches, all of which weaken correlations with biomass (Zhao et al., 2016; Ma et al., 2020).

Among the indices tested, EVI in November had the highest correlation with AGB. This discovery is consistent with Huete et al. (2002), who demonstrated that EVI is less sensitive than NDVI to soil background and air scattering effects, both of which affect Landsat optical data, resulting in a more accurate proxy of canopy structure and biomass in dense forests. The superior performance of EVI in this study highlights its utility in densely vegetated landscapes where NDVI may saturate or be distorted by understory and soil reflectance (Huete et al., 2002; Jiang et al., 2020). NDVI also exhibited strong correlations, reflecting its sensitivity to canopy greenness and LAI peaks (Carlson & Ripley, 1997), though its effectiveness diminishes in dense forests due to saturation above certain biomass levels (Myneni et al., 1995; Lu et al., 2016). NBR also showed notable correlations, reflecting the importance of shortwave infrared (SWIR) bands available in Landsat sensors, as it contrasts near-infrared and shortwave-infrared reflectance, which are sensitive to vegetation water content and canopy structure (Pontes-Lopes et al., 2022). These spectral properties make NBR valuable for capturing biomass-related variation, compared to purely red-NIR indices. Zheng et al. (2007) also demonstrated shortwave infrared band as satisfactory biomass estimator in forests characterized by high canopy density.

Beyond phenology, several operational and data-related factors can influence the strength of VI–AGB relationships across seasons and provide opportunities for improvement in future studies. Optimising image acquisition timing to coincide with seasonal periods when canopy greenness and structure maximise spectral sensitivity to biomass, which for many forests occurs near, but not necessarily at, peak canopy vigour, can improve VI–AGB relationships (Zhu & Liu, 2015; Zhao et al., 2016). The use of higher-temporal-resolution optical sensors, such as Sentinel-2, increases flexibility in selecting optimal dates and filling cloud-related gaps, improving the match between field measurements and satellite observations (Poudel et al., 2023). Additionally, integrating complementary structural information from LiDAR or radar (SAR) data could help capture canopy height and volume; key biomass components that optical indices alone may not fully represent, particularly in dense forests (Lefsky et al., 2002; Mitchard et al., 2012). Although such integration extends beyond simple correlation analysis, it represents a logical pathway for refining biomass estimation accuracy.

5.3. Model Performance Across Approaches and Seasonal Scenarios

This study compared the predictive performance of linear regression, quadratic regression, and Random Forest (RF) models for estimating above-ground biomass (AGB) in Kankali Community Forest (CF) using Landsat-derived vegetation indices (NDVI, EVI, NBR) across four seasonal scenarios: combined March and November data, November-only, March-only, and a March-only temporal transferability test using 2025 imagery. The findings reveal a clear pattern driven by both algorithm choice and seasonal data selection.

All models discussed in this section were fitted using square root–transformed biomass, selected after preliminary testing showed it improved model accuracy ($R^2 = 0.694$, RMSE ≈ 82.9) compared to untransformed and log-transformed data. This transformation stabilized variance and improved residual normality without over-compressing high values, thereby providing a reliable basis for comparing seasonal and algorithmic performance (Long & Ervin, 2000; Pretzsch, 2009; Dunn & Smyth, 2018; Cysneiros et al., 2020).

Across all scenarios, RF model consistently demonstrated superior predictive power compared to parametric linear and quadratic regression models. In the combined March + November multi-season scenario, RF achieved an $R^2 = 0.94$ for training and 0.62 for testing, substantially outperforming linear and quadratic regressions which yielded test R^2 values of approximately 0.58. This outcome aligns well with the broadly recognized strengths of ensemble machine learning methods in remote sensing biomass estimation, particularly their adeptness at capturing complex nonlinear relationships, managing multicollinearity among correlated predictors, and accommodating interactions that parametric models inherently struggle with (Breiman, 2001; Mutanga et al., 2004; Belgiu & Drăguţ, 2016). Similar trends have been reported in subtropical Nepalese forests, where RF has achieved $R^2 \geq 0.81$ with Sentinel-2 predictors (Pandit et al., 2020) compared to ~0.56 for multiple linear regression. In tropical systems, Sinha et al. (2015) likewise documented R^2 gains of 0.1–0.2 over regression methods when combining Landsat and LiDAR inputs with RF.

When exploring the role of seasonal data composition, the models built exclusively on November imagery displayed slightly greater accuracy than those combining March and November inputs within the parametric frameworks. In linear regression, November-only inputs achieved an R^2 of 0.666 and an RMSE of approximately 84 $t \cdot ha^{-1}$, outperforming combined-season models (R^2 = 0.580). Quadratic regressions produced a similar pattern (R^2 = 0.694 vs. 0.580). Meanwhile, RF performance was nearly identical for the two seasonal input sets, indicating that while RF benefits marginally from March data, the dominant spectral signal arises from post-monsoon imagery corresponding to November. This spectral dominance likely reflects that the post-monsoon canopies in *Shorea robusta* dominated forests typically exhibit maximum leaf area, chlorophyll content, and intact structure, producing high red-band absorption and strong NIR reflectance (Carlson & Ripley, 1997; Huete et al., 2002). Comparable seasonal performance patterns have been reported in other subtropical and tropical forests: Zhao et al. (2016) and Ma et al. (2020) found that imagery acquired in post-rainy or autumn periods yielded the strongest VI–AGB correlations, while late dry-season data produced substantially weaker relationships, a result they attributed to canopy senescence and increased background signal from soil and litter. Notably, November EVI and NBR held the greatest predictive importance in RF models and exhibited the strongest coefficients in regression analyses, a finding consistent with Zhao et al. (2016), who reported EVI's robustness in dense canopies and NBR's sensitivity to canopy moisture and structural attributes.

In contrast, March-only models consistently underperformed regardless of the modelling approach. Even though RF training accuracy was relatively high (R^2 = 0.851, RMSE ≈ 64), the test R^2 dropped to only ~0.21 (RMSE > 110 $t \cdot ha^{-1}$), and regression methods also performed poorly (linear R^2 = 0.330). The poorest results came from quadratic regression (R^2 = 0.075, RMSE = 122 $t \cdot ha^{-1}$). This poor generalization underscores the inherent limitations posed by dry-season imagery, when leaf senescence, canopy thinning, and high background reflectance from soil and litter compress VI dynamic ranges and inject noise (Zhao et al., 2016; Ma et al., 2020). The instability of March-only models was most apparent in the temporal transferability test, where models trained on earlier years failed to predict 2025 biomass accurately, a behavior consistent with literature noting that VI–AGB relationships during sub-optimal phenological windows are more sensitive to inter-annual variation (Fassnacht et al., 2014).

The seasonal performance ranking observed here: November outperforming combined-season, which in turn outperforms March-only, is consistent with prior remote sensing and ecological studies. While Powell et al. (2010), Avitabile et al. (2012) and Zhu & Liu (2015), have shown that integrating multiple phenological phases enhances biomass estimation by mitigating saturation effects and leveraging complementary canopy structural signals, our findings suggest that the phenological value of March data in this ecosystem is comparatively marginal. The limited gain from March in our case likely reflects the absence of complementary biomass-related cues in late-dry imagery for this forest type. It is plausible that early-season imagery capturing leaf flush or initial canopy expansion, rather than late dry-season imagery, might provide more complementary biomass information when combined with peak-season data, an approach that has demonstrated benefits in temperate and savanna ecosystems (Heiskanen, 2006). This suggests considering testing alternative seasonal combinations such as early + peak imagery to potentially improve estimation accuracy.

Algorithm comparison also requires nuance. While RF was clearly optimal for our objective of minimizing prediction error, there is broad agreement in the literature that no single method is universally "best"; choice depends on study goals, data characteristics, and trade-offs between accuracy, bias, and interpretability (Powell et al., 2010; Zhu & Liu, 2015). For example, reduced model complexity in linear regression can be valuable where interpretability or bias minimization matter more than absolute error reduction. Our results therefore align with a context-dependent view: RF is superior here for predictive accuracy, but not inherently the best in all biomass mapping applications.

5.4. Influence of Elevation and Climatic Variables on Biomass Estimation

Incorporating elevation and monthly climatic variables (mean temperature, precipitation, and potential evapotranspiration) into the multi-season vegetation index model for Kankali CF did not materially improve predictive accuracy. The linear model with these ancillary predictors achieved a test R2=0.574 and RMSE = 85.9 t ha^{-1}, almost identical to the multi-season vegetation indices model (R2=0.580; RMSE = 84.6 t ha^{-1}). This near-equivalence indicates that, under the present data conditions, the added topographic and climate variables contributed little new explanatory information.

Topographic and climatic covariates are recognized as potentially important drivers of forest biomass patterns because they influence energy balance, water availability, and site productivity (Salinas-Melgoza et al., 2018; Mehmood et al., 2024). In landscapes with large environmental gradients or heterogeneous vegetation types, such variables can significantly improve biomass estimates. However, multiple studies have also documented cases where ancillary environmental variables had only a marginal effect on model fit, particularly when the spatial range in those variables was limited or when fine-scale remote sensing metrics already integrated much of their influence. Guitet et al. (2015), for example, analyzed over 2,500 tropical forest plots in French Guiana and found that environmental variables accounted for only a minor proportion of biomass variation at the landscape scale; weak spatial autocorrelation and limited environmental gradients constrained any accuracy gains from their inclusion.

The limited gain in Kankali CF is consistent with these findings. The forest occupies a relatively narrow elevational band (220–580 m a.s.l.) within a single lowland *Shorea robusta* forest type. Over this range, microclimatic and edaphic differences are modest, so a strong, monotonic biomass–elevation relationship is unlikely. In contrast, if the forest extended upslope into montane zones (> 3,000 m), a pronounced decline in biomass with elevation would be expected, as observed by Girardin et al. (2014) along six tropical Andean transects, where above-ground biomass decreased from 247 Mg ha^{-1} at 210 m to 86 Mg ha^{-1} at 3,450 m.

Overall, our results align with the broader body of work showing that in relatively homogeneous, low-relief tropical forests, coarse-scale environmental variables tend to contribute more to ecological interpretation than to purely predictive accuracy when combined with robust spectral indices (Lu, 2006; Guitet et al., 2015). Similarly, the climate data used here came from the CRU TS dataset at ~0.5° spatial resolution, providing broad-scale, monthly means rather than local, event-scale measurements. Such coarse surfaces are valuable for representing inter-annual climate patterns consistently, but they cannot capture microclimatic differences within the forest. In Kankali CF, the multi-season NDVI, EVI, and NBR predictors appear to have already captured the dominant canopy signals related to biomass, leaving little residual variation for ancillary topographic and coarse climate data to explain.

6. Conclusion

This study demonstrates that integrating multi-seasonal Landsat vegetation indices with robust machine learning techniques offers a reliable, scalable, and operationally feasible approach to estimating aboveground biomass (AGB) in subtropical community forests. Over the past two decades, Kankali Community Forest (CF) has experienced substantial and sustained increases in biomass, reflecting the effectiveness of Nepal's community forestry program under regulated selection harvesting. This positive trend underscores the dual ecological and climate benefits of long-term, community-led forest stewardship.

Empirical results show that post-monsoon (November) vegetation indices, particularly the EVI, are consistently stronger predictors of AGB than dry season indices, reflecting the critical role of phenological conditions in remote sensing-based biomass assessment. Among the evaluated empirical models, the Random Forest approach consistently outperformed linear and quadratic regression models, capturing complex nonlinear relationships between spectral predictors and biomass. Linear and quadratic regressions, while interpretable, proved limited in their ability to account for the inherent variability and nonlinearities present in multi-temporal, multispectral remote sensing data. Seasonal model comparisons confirmed that

November-only datasets achieved equal or superior predictive performance to multi-seasonal datasets in parametric models, while March-only models were markedly less accurate and demonstrated poor temporal transferability. For Random Forest, November-only and multi-season datasets produced similar results, indicating that seasonal differences are less pronounced in flexible non-parametric frameworks.

On the contrary, the inclusion of ancillary elevation and country-level climate variables did not yield substantial improvements in model accuracy compared to models based solely on vegetation indices. This was likely due to the coarse spatial resolution of the climate data forest's narrow environmental gradients and homogenous composition and the strong explanatory power of vegetation indices alone.

Ultimately, this study reinforces the value and feasibility of satellite-based, empirical, and machine learning approaches for forest biomass monitoring within Nepal and similar subtropical ecological zones. From a policy perspective, these findings provide actionable methodological insight for national forest inventories and REDD+ initiatives, particularly in leveraging multi-seasonal satellite archives and advanced modeling for operational, repeatable and cost-effective carbon stock assessments, strengthening the scientific basis for climate change mitigation strategies, carbon accounting, and sustainable forest management planning.

Building on this work, future research should explore seasonal combinations beyond March and November, such as early leaf-flush or peak canopy periods, to assess their complementarity for biomass estimation. Integrating optical indices with LiDAR or radar data would allow canopy height, volume, and vertical complexity to be captured more comprehensively, while the use of higher-resolution microclimatic, edaphic, and topographic datasets could help explain fine-scale biomass variation. Testing this framework across diverse forest types, ecological zones, and management regimes will provide valuable insights into its transferability and scalability. Advancing these approaches will help ensure that biomass monitoring becomes increasingly accurate, operationally robust, and directly supportive of sustainable forest management and climate change mitigation in dynamic and heterogeneous forest systems.

Reference:

Aasen, H., Burkart, A., Bolten, A., & Bareth, G. (2015). Generating 3D hyperspectral information with lightweight UAV snapshot cameras for vegetation monitoring: From camera calibration to quality assurance. *ISPRS Journal of Photogrammetry and Remote Sensing, 108*, 245-259.

Ahmad, N., Ullah, S., Zhao, N., Mumtaz, F., Ali, A., Ali, A., ... & Shakir, M. (2023). Comparative analysis of remote sensing and geo-statistical techniques to quantify forest biomass. *Forests, 14*(2), 379.

Alexandrov, G. A. (2007). Carbon stock growth in a forest stand: The power of age. *Carbon Balance and Management, 2*(1), 1–5. https://doi.org/10.1186/1750-0680-2-4

Almalki, R., Khaki, M., Saco, P. M., & Rodriguez, J. F. (2022). Monitoring and mapping vegetation cover changes in arid and semi-arid areas using remote sensing technology: A review. *Remote Sensing, 14*(20), 5143.

Anees, A., Aryal, J., & O'Reilly, M. M. (2024). Improving aboveground biomass estimation using multi-temporal Landsat data in temperate forests. *Remote Sensing of Environment, 300*, 113–125.

Anees, S. A., Mehmood, K., Khan, W. R., Sajjad, M., Alahmadi, T. A., Alharbi, S. A., & Luo, M. (2024). Integration of machine learning and remote sensing for above ground biomass estimation through Landsat-9 and field data in temperate forests of the Himalayan region. *Ecological Informatics, 82*, 102732.

Avitabile, V., Baccini, A., Friedl, M. A., & Schmullius, C. (2012). Capabilities and limitations of Landsat and land cover data for aboveground woody biomass estimation of Uganda. *Remote Sensing of Environment, 117*, 366-380.

Bachmann, F., Herbst, R., Gebbers, R., & Hafner, V. V. (2013). Micro UAV based georeferenced orthophoto generation in VIS+ NIR for precision agriculture. *The International Archives of the Photogrammetry, Remote Sensing and Spatial Information Sciences, 40*, 11–16.

Bajracharya, R. M., Lal, R., & Kimble, J. M. (2018). Soil organic carbon distribution in aggregates and primary particle fractions as influenced by erosion phases and landscape position. In *Soil processes and the carbon cycle* (pp. 353–367). CRC Press.

Baral, S. K., Malla, R., & Ranabhat, S. (2009). Above-ground carbon stock assessment in different forest types of Nepal. *Banko Janakari, 19*(2), 10–14.

Baral, S., & Vacik, H. (2018). What governs tree harvesting in community forestry—regulatory instruments or forest bureaucrats' discretion? *Forests, 9*, 649. https://doi.org/10.3390/f9100649

Baral, S., Neumann, M., Joshi, K. P., Basnyat, B., & Vacik, H. (2025). Exploring the implications of selective harvesting for forest dynamics: A longitudinal analysis of Sal dominated community forests. *Trees, Forests and People, 20*, 100832.

Behera, S. K., Sahu, N., Mishra, A. K., Bargali, S. S., Behera, M. D., & Tuli, R. (2017). Aboveground biomass and carbon stock assessment in Indian tropical deciduous forest and relationship with stand structural attributes. *Ecological Engineering, 99*, 513–524. https://doi.org/10.1016/j.ecoleng.2016.11.002

Belgiu, M., & Drăguţ, L. (2016). Random forest in remote sensing: A review of applications and future directions. *ISPRS Journal of Photogrammetry and Remote Sensing, 114*, 24–31.

Breiman, L. (2001). Random forests. *Machine Learning, 45*, 5–32.

Brown, S., Gillespie, A. J., & Lugo, A. E. (1989). Biomass estimation methods for tropical forests with applications to forest inventory data. *Forest Science, 35*(4), 881–902.

Canadell, J. G., & Raupach, M. R. (2008). Managing forests for climate change mitigation. *Science, 320*(5882), 1456–1457. https://doi.org/10.1126/science.1155422

Candiago, S., Remondino, F., De Giglio, M., Dubbini, M., & Gattelli, M. (2015). Evaluating multispectral images and vegetation indices for precision farming applications from UAV images. *Remote Sensing, 7*(4), 4026–4047.

Carlson, T. N., & Ripley, D. A. (1997). On the relation between NDVI, fractional vegetation cover, and leaf area index. *Remote Sensing of Environment, 62*(3), 241–252.

Chave, J., Réjou-Méchain, M., Búrquez, A., Chidumayo, E., Colgan, M. S., Delitti, W. B., ... & Vieilledent, G. (2014). Improved allometric models to estimate the aboveground biomass of tropical trees. *Global Change Biology, 20*(10), 3177–3190.

Cheng, W., Yang, C., Zhou, J., Zhou, W., & Liu, Y. (2009). Research summary of forest volume quantitative estimation based on remote sensing technology. *Journal of Anhui Agricultural Sciences, 37*, 7746–7750.

Cho, M. A., Skidmore, A., Corsi, F., Van Wieren, S. E., & Sobhan, I. (2007). Estimation of green grass/herb biomass from airborne hyperspectral imagery using spectral indices and partial least squares regression. *International Journal of Applied Earth Observation and Geoinformation, 9*(4), 414–424.

Cohen, W. B., & Goward, S. N. (2004). Landsat's role in ecological applications of remote sensing. *Bioscience, 54*, 535–545.

Curtis, R. O. (1967). Height-diameter and height-diameter-age equations for second-growth Douglas-fir. *Forest Science, 13*(4), 365–375.

Cutler, M. E. J., Boyd, D. S., Foody, G. M., & Vetrivel, A. (2012). Estimating tropical forest biomass with a combination of SAR image texture and Landsat TM data: An assessment of predictions between regions. *ISPRS Journal of Photogrammetry and Remote Sensing, 70*, 66–77. https://doi.org/10.1016/j.isprsjprs.2012.03.011

Cysneiros, V. C., Gaui, T. D., Silveira Filho, T. B., Pelissari, A. L., Machado, S. D. A., Carvalho, D. C., & Amorim, H. B. (2020). Tree volume modeling for forest types in the Atlantic Forest: Generic and specific models. *iForest (Viterbo), 13*(5), 417–425. http://dx.doi.org/10.3832/ifor3495-013

Dar, J. A., Rather, M. Y., Subashree, K., Sundarapandian, S., & Khan, M. L. (2017). Distribution patterns of tree, understorey, and detritus biomass in coniferous and broad-leaved forests of Western Himalaya, India. *Journal of Sustainable Forestry, 36*(8), 787–805. https://doi.org/10.1080/10549811.2017.1363055

Drake, J. B., Knox, R. G., Dubayah, R. O., Clark, D. B., Condit, R., Blair, J. B., & Hofton, M. (2003). Above-ground biomass estimation in closed canopy Neotropical forests using lidar remote sensing: Factors affecting the generality of relationships. *Global Ecology and Biogeography, 12*(2), 147–159.

du Plessis, W. P. (1999). Linear regression relationships between NDVI, vegetation and rainfall in Etosha National Park, Namibia. *Journal of Arid Environments, 42*(3), 235–260.

Du, H., Zhou, G., Ge, H., Fan, W., Xu, X., Fan, W., & Shi, Y. (2012). Satellite-based carbon stock estimation for bamboo forest with a non-linear partial least square regression technique. *International Journal of Remote Sensing, 33*(5), 1139–1159. https://doi.org/10.1080/01431161.2011.603379

Dube, T., & Mutanga, O. (2015). Evaluating the utility of the medium-spatial resolution Landsat 8 multispectral sensor in quantifying aboveground biomass. *ISPRS Journal of Photogrammetry and Remote Sensing, 101*, 36–46.

Dunn, P. K., & Smyth, G. K. (2018). *Generalized linear models with examples in R* (573 p.). Springer. http://dx.doi.org/10.1007/978-1-4419-0118-7

Dymond, C. C., Mladenoff, D. J., & Radeloff, V. C. (2002). Phenological differences in Tasseled Cap indices improve deciduous forest classification. *Remote Sensing of Environment, 80*(3), 460–472.

Fahey, T. J., Woodbury, P. B., Battles, J. J., Goodale, C. L., Hamburg, S. P., Ollinger, S. V., & others. (2010). Forest carbon storage: Ecology, management, and policy. *Frontiers in Ecology and the Environment, 8*(5), 245–252. https://doi.org/10.1890/090200

Fassnacht, F. E., Hartig, F., Latifi, H., Berger, C., Hernández, J., Corvalán, P., & Koch, B. (2014). Importance of sample size, data type and prediction method for remote sensing-based estimations of aboveground forest biomass. *Remote Sensing of Environment, 154*, 102–114.

Food and Agriculture Organization of the United Nations. (2011). *FAO glossary of terms*. FAO. https://www.fao.org accessed February 2, 2016

Foody, G. M., et al. (2003). Nonlinearity in biomass estimation models for tropical forests. *International Journal of Remote Sensing, 24*(9), 1947–1966.

Forest Research and Training Centre. (2022). *Terai forests of Nepal: Forest inventory report* [PDF]. Ministry of Forests and Environment, Nepal.

Forsell, N., Korosuo, A., Federici, S., Gusti, M., Rincón-Cristóbal, J. J., Rüter, S., & Gardiner, J. (2018). *Guidance on developing and reporting the forest reference levels in accordance with Regulation (EU) 2018/841*. European Commission.

Gasparri, N. I., Parmuchi, M. G., Bono, J., Karszenbaum, H., & Montenegro, C. L. (2010). Assessing multi-temporal Landsat 7 ETM+ images for estimating above-ground biomass in subtropical dry forests of Argentina. *Journal of Arid Environments, 74*, 1262–1270.

Geipel, J., Link, J., Wirwahn, J. A., & Claupein, W. (2016). A programmable aerial multispectral camera system for in-season crop biomass and nitrogen content estimation. *Agriculture, 6*(1), 4.

Gibbs, H. K., Brown, S., Niles, J. O., & Foley, J. A. (2007). Monitoring and estimating tropical forest carbon stocks: Making REDD a reality. *Environmental Research Letters, 2*(4). https://doi.org/10.1088/1748-9326/2/4/045023

Girardin, C. A., Farfan-Rios, W., Garcia, K., Feeley, K. J., Jørgensen, P. M., Murakami, A. A., & Malhi, Y. (2014). Spatial patterns of above-ground structure, biomass and composition in a network of six Andean elevation transects. *Plant Ecology & Diversity, 7*(1–2), 161–171.

Gitelson, A. A., & Merzlyak, M. N. (1997). Remote estimation of chlorophyll content in higher plant leaves. *International Journal of Remote Sensing, 18*(12), 2691–2697. https://doi.org/10.1080/014311697217558

Goetz, S. J., & Dubayah, R. (2011). Advances in remote sensing technology and implications for measuring and monitoring forest carbon stocks and change. *Carbon Management, 2*(3), 231–244.

Grassroot Global. (2017). *Case studies: Community based forest enterprises*. Grassroot Global. https://www.grassrootsglobal.net/mer2020/pdf_files/3.1_doc_sita.pdf

Guitet, S., Hérault, B., Molto, Q., Brunaux, O., & Couteron, P. (2015). Spatial structure of above-ground biomass limits accuracy of carbon mapping in rainforest but large scale forest inventories can help to overcome. *PLoS One, 10*(9), e0138456.

Harishma, K. M., Sandeep, S., & Sreekumar, V. B. (2020). Biomass and carbon stocks in mangrove ecosystems of Kerala, southwest coast of India. *Ecological Processes, 9*(1), 1–9. https://doi.org/10.1186/s13717-020-00212-5

Harris, I., Osborn, T. J., Jones, P., & Lister, D. (2020). Version 4 of the CRU TS monthly high-resolution gridded multivariate climate dataset. *Scientific Data, 7*(1), 109. https://doi.org/10.1038/s41597-020-0453-3

Heiskanen, J. (2006). Estimating aboveground tree biomass and leaf area index in a mountain birch forest using ASTER satellite data. *International Journal of Remote Sensing, 27*(6), 1135–1158.

Henry, M., Picard, N., Trotta, C., Manlay, R. J., Valentini, R., Bernoux, M., & Saint-André, L. (2011). Estimating tree biomass of Sub-Saharan African forests: A review of available allometric equations. *45*(January), 39.

Hojo, A., Avtar, R., Nakaji, T., Tadono, T., & Takagi, K. (2023). Modeling forest aboveground biomass using freely available satellite and multisource datasets. *Ecological Informatics, 74,* 101973. https://doi.org/10.1016/j.ecoinf.2023.101973

Houghton, R. A., Hall, F., & Goetz, S. J. (2009). Importance of biomass in the global carbon cycle. *Journal of Geophysical Research: Biogeosciences, 114*(G00D06), 1–13. https://doi.org/10.1029/2009JG000935

Huete, A., Didan, K., Miura, T., Rodriguez, E. P., Gao, X., & Ferreira, L. G. (2002). Overview of the radiometric and biophysical performance of the MODIS vegetation indices. *Remote Sensing of Environment, 83*(1–2), 195–213.

Ingram, J. C., Dawson, T. P., & Whittaker, R. J. (2005). Mapping tropical forest structure in southeastern Madagascar using remote sensing and artificial neural networks. *Remote Sensing of Environment, 94*(4), 491–507.

IPCC. (2006). *2006 IPCC guidelines for national greenhouse inventories – A primer*. National Greenhouse Gas Inventories Programme.

Ismail, I., Sohail, M., Gilani, H., Ali, A., Hussain, K., Hussain, K., Karky, B., Qamer, F., Qazi, W., & Ning, W. (2018). Forest inventory and analysis in Gilgit-Baltistan: A contribution towards developing a forest inventory for all Pakistan. *International Journal of Climate Change Strategies and Management, 10*(4), 616–631.

Jiang, F., Kutia, M., Ma, K., Chen, S., Long, J., & Sun, H. (2021). Estimating the aboveground biomass of coniferous forest in Northeast China using spectral variables, land surface temperature, and soil moisture. *Science of the Total Environment, 785,* 147335. https://doi.org/10.1016/j.scitotenv.2021.147335

Karki, S., Joshi, N. R., & Udas, E. (2016). Assessment of forest carbon stock and carbon sequestration rates at the ICIMOD Knowledge Park in Godavari: The Himalayan Climate Change Adaptation Programme (HICAP). *ResearchGate.* https://www.researchgate.net/publication/310597175

Kauranne, T., Joshi, A., Gautam, B., Manandhar, U., Nepal, S., Peuhkurinen, J., Hämäläinen, J., Junttila, V., Gunia, K., Latva-Käyrä, P., et al. (2017). LiDAR-assisted multi-source program (LAMP) for measuring aboveground biomass and forest carbon. *Remote Sensing, 9*(2), 154. https://doi.org/10.3390/rs9020154

KC, Y. B., Liu, Q., Saud, P., Gaire, D., & Adhikari, H. (2024). Estimation of above-ground forest biomass in Nepal by the use of airborne LiDAR and forest inventory data. *Land, 13*(2). https://doi.org/10.3390/land13020213

Ketterings, Q. M., Coe, R., Van Noordwijk, M., Ambagau', Y., & Palm, C. A. (2001). Reducing uncertainty in the use of allometric biomass equations for predicting above-ground tree biomass in mixed secondary forests. *Forest Ecology and Management, 146*(1–3), 199–209. https://doi.org/10.1016/S0378-1127(00)00460-6

Khallaf, M. (2011). The impact of air pollution on health, economy, environment and agricultural sources. *Tech Europe University Campus STeP R.*

Khanna, L. S., & Chaturvedi, A. N. (1982). *Forest mensuration*. International Book Distributors.

Lefsky, M. A., Cohen, W. B., Parker, G. G., & Harding, D. J. (2002). Lidar remote sensing for ecosystem studies. *BioScience, 52*(1), 19–30. https://doi.org/10.1641/0006-3568(2002)052[0019:LRSFES]2.0.CO;2

Li, M., Tan, Y., Pan, J., & Peng, S. (2008). Modeling forest aboveground biomass by combining spectrum, textures and topographic features. *Frontiers of Forestry in China, 3*(1), 10–15.

Li, Y., Li, M., Li, C., & Liu, Z. (2020). Forest aboveground biomass estimation using Landsat 8 and Sentinel-1A data with machine learning algorithms. *Scientific Reports, 10*(1), 9952. https://doi.org/10.1038/s41598-020-66896-2

Long, J. S., & Ervin, L. H. (2000). Using heteroscedasticity consistent standard errors in the linear regression model. *The American Statistician, 54*(3), 217–224. https://doi.org/10.1080/00031305.2000.10474549

Lu, D. (2006). The potential and challenge of remote sensing–based biomass estimation. *International Journal of Remote Sensing, 27*(7), 1297–1328. https://doi.org/10.1080/01431160500486732

Lu, D., Chen, Q., Wang, G., Liu, L., Li, G., & Moran, E. (2016). A survey of remote sensing-based aboveground biomass estimation methods in forest ecosystems. *International Journal of Digital Earth, 9*(1), 63–105. https://doi.org/10.1080/17538947.2015.1051656

Lu, D., Chen, Q., Wang, G., Moran, E., Batistella, M., Zhang, M., Vaglio Laurin, G., & Saah, D. (2012). Aboveground forest biomass estimation with Landsat and LiDAR data and uncertainty analysis of the estimates. *International Journal of Forestry Research, 2012,* 16. https://doi.org/10.1155/2012/416936

Ma, A., Miao, Z., Xie, L., Tian, J., Zhao, X., & Dong, L. (2025). Integrating climate and soil factors enhances biomass estimation for natural white birch (*Betula platyphylla* Sukaczev). *Frontiers in Forests and Global Change, 8,* 1549531. https://doi.org/10.3389/ffgc.2025.1549531

Main-Knorn, M., Cohen, W. B., Kennedy, R. E., Grodzki, W., Pflugmacher, D., Griffiths, P., & Hostert, P. (2013). Monitoring coniferous forest biomass change using a Landsat trajectory-based approach. *Remote Sensing of Environment, 139,* 277–290. https://doi.org/10.1016/j.rse.2013.07.019

Malhi, Y., Meir, P., & Brown, S. (2002). Forests, carbon and global climate. *Philosophical Transactions of the Royal Society A: Mathematical, Physical and Engineering Sciences, 360*(1797), 1567–1591. https://doi.org/10.1098/rsta.2002.1045

Maynard, C. L., Lawrence, R. L., Nielsen, G. A., & Decker, G. (2007). Modeling vegetation amount using bandwise regression and ecological site descriptions as an alternative to vegetation indices. *GIScience & Remote Sensing, 44*(1), 68–81. https://doi.org/10.2747/1548-1603.44.1.68

Mehmood, K., Anees, S. A., Rehman, A., Pan, S., Tariq, A., Zubair, M., ... & Luo, M. (2024). *Exploring spatiotemporal dynamics of NDVI and climate-driven responses in ecosystems: insights for sustainable management and climate resilience. Ecol Inform 80: 102532*.

Mitchard, E. T., Saatchi, S. S., White, L. J., Abernethy, K. A., Jeffery, K. J., Lewis, S. L., … Meir, P. (2012). Mapping tropical forest biomass with radar and spaceborne LiDAR in Lopé National Park, Gabon: Overcoming problems of high biomass and persistent cloud. *Biogeosciences, 9*(1), 179–191. https://doi.org/10.5194/bg-9-179-2012

Muhammad, B., Rehman, A. U., Mumtaz, F., Qun, Y., & Zhongkui, J. (2024). Estimation of above-ground biomass in dry temperate forests using Sentinel-2 data and random forest: A case study of the Swat area of Pakistan. *Frontiers in Environmental Science, 12,* 1448648. https://doi.org/10.3389/fenvs.2024.1448648

Müller, W. G. (2001). *Collecting spatial data: Optimum design of experiments for random fields*. Physica-Verlag.

Musthafa, M., & Singh, G. (2022). Multi-sensor fusion for improved biomass mapping: Integrating SAR, LiDAR, and optical remote sensing. *Ecological Informatics, 68,* 101–115. https://doi.org/10.1016/j.ecoinf.2022.101115

Mutanga, O., & Skidmore, A. K. (2004). Hyperspectral band depth analysis for a better estimation of grass biomass (*Cenchrus ciliaris*) measured under controlled laboratory conditions. *International Journal of Applied Earth Observation and Geoinformation, 5*(2), 87–96. https://doi.org/10.1016/j.jag.2004.01.002

Myneni, R. B., Hall, F. G., Sellers, P. J., & Marshak, A. L. (1995). The interpretation of spectral vegetation indexes. *IEEE Transactions on Geoscience and Remote Sensing, 33*(2), 481–486. https://doi.org/10.1109/36.377084

Pan, Y., Birdsey, R. A., Phillips, O. L., & Jackson, R. B. (2013). The structure, distribution, and biomass of the world's forests. *Annual Review of Ecology, Evolution, and Systematics, 44,* 593–622. https://doi.org/10.1146/annurev-ecolsys-110512-135914

Pandit, S., Tsuyuki, S., & Dube, T. (2018). Estimating above-ground biomass in sub-tropical buffer zone community forests, Nepal, using Sentinel 2 data. *Remote Sensing, 10*(4). https://doi.org/10.3390/rs10040601

Pandit, S., Tsuyuki, S., & Dube, T. (2020). Exploring the inclusion of Sentinel-2 MSI texture metrics in above-ground biomass estimation in the community forest of Nepal. *Geocarto International, 35*(16), 1832–1849. https://doi.org/10.1080/10106049.2019.1588390

Patenaude, G., Milne, R., & Dawson, T. P. (2005). Synthesis of remote sensing approaches for forest carbon estimation: Reporting to the Kyoto Protocol. *Environmental Science & Policy, 8*(2), 161–178. https://doi.org/10.1016/j.envsci.2004.12.010

Pontes-Lopes, A., Dalagnol, R., Dutra, A. C., de Jesus Silva, C. V., de Alencastro Graça, P. M. L., & de Oliveira e Cruz de Aragão, L. E. (2022). Quantifying post-fire changes in the aboveground biomass of an Amazonian forest based on field and remote sensing data. *Remote Sensing, 14*(7), 1545. https://doi.org/10.3390/rs14071545

Porté, A., & Bartelink, H. H. (2002). Modelling mixed forest growth: A review of models for forest management. *Ecological Modelling, 150*(1–2), 141–188. https://doi.org/10.1016/S0304-3800(01)00476-8

Poudel, A., Shrestha, H. L., Mahat, N., Sharma, G., Aryal, S., Kalakheti, R., & Lamsal, B. (2023). Modeling and mapping of aboveground biomass and carbon stock using Sentinel-2 imagery in Chure region, Nepal. *International Journal of Forestry Research, 2023,* 5553957. https://doi.org/10.1155/2023/5553957

Powell, S. L., Cohen, W. B., Healey, S. P., Kennedy, R. E., Moisen, G. G., Pierce, K. B., & Ohmann, J. L. (2010). Quantification of live aboveground forest biomass dynamics with Landsat time-series and field inventory data: A comparison of empirical modeling approaches. *Remote Sensing of Environment, 114*(5), 1053–1068. https://doi.org/10.1016/j.rse.2010.01.017

Pretzsch, H. (2009). *Forest dynamics, growth and yield: From measurement to model* (664 p.). Berlin: Springer. https://doi.org/10.1007/978-3-540-88307-4

Puri, L., Meilby, H., Rayamajhi, S., Timilsina, Y. P., Gautam, N. P., Subedi, R., & Larsen, H. O. (2012). Growth and volume based on permanent sample plots in forests managed by communities. *Banko Janakari, 22*(2), 11–18.

Ravindranath, N. H., & Ostwald, M. (2007). *Carbon inventory methods: Handbook for greenhouse gas inventory, carbon mitigation and roundwood production projects* (Vol. 29). Springer Science & Business Media.

Rozendaal, D. M. A., Requena Suarez, D., De Sy, V., Avitabile, V., Carter, S., Adou Yao, C. Y., Alvarez-Davila, E., Anderson-Teixeira, K., Araujo-Murakami, A., Arroyo, L., Barca, B., Baker, T. R., Birigazzi, L., Bongers, F., Branthomme, A., Brienen, R. J. W., Carreiras, J. O. M. B., Cazzolla Gatti, R., Cook-Patton, S. C., … Herold, M. (2022). Aboveground forest biomass varies across continents, ecological zones and successional stages: Refined IPCC default values for tropical and subtropical forests. *Environmental Research Letters, 17*(1). https://doi.org/10.1088/1748-9326/ac45b3

Saatchi, S. S., Harris, N. L., Brown, S., Lefsky, M., Mitchard, E. T. A., Salas, W., … Morel, A. (2011). Benchmark map of forest carbon stocks in tropical regions across three continents. *Proceedings of the National Academy of Sciences, 108*(24), 9899–9904. https://doi.org/10.1073/pnas.1019576108

Salinas-Melgoza, M. A., Skutsch, M., & Lovett, J. C. (2018). Predicting aboveground forest biomass with topographic variables in human-impacted tropical dry forest landscapes. *Ecosphere, 9,* e02063. https://doi.org/10.1002/ecs2.2063

Sileshi, G. W. (2014). A critical review of forest biomass estimation models, common mistakes and corrective measures. *Forest Ecology and Management, 329,* 237–254. https://doi.org/10.1016/j.foreco.2014.05.034

Sinha, S., Jeganathan, C., Sharma, L. K., & Nathawat, M. S. (2015). A review of radar remote sensing for biomass estimation. *International Journal of Environmental Science and Technology, 12*(5), 1779–1792. https://doi.org/10.1007/s13762-015-0750-0

Somogyi, Z., Cienciala, E., Mäkipää, R., Muukkonen, P., Lehtonen, A., & Weiss, P. (2007). Indirect methods of large-scale forest biomass estimation. *European Journal of Forest Research, 126*(2), 197–207. https://doi.org/10.1007/s10342-006-0125-7

Soto-Navarro, C., Ravilious, C., Arnell, A., De Lamo, X., Harfoot, M., Hill, S. L. L., Wearn, O. R., Santoro, M., Bouvet, A., Mermoz, S., Le Toan, T., Xia, J., Liu, S., Yuan, W., Spawn, S. A., Gibbs, H. K., Ferrier, S., Harwood, T., Alkemade, R., … Kapos, V. (2020). Mapping co-benefits for carbon storage and biodiversity to inform conservation policy and action. *Philosophical Transactions of the Royal Society B: Biological Sciences, 375*(1794). https://doi.org/10.1098/rstb.2019.0128

Suryawanshi, M., Patel, A. R., Kale, T. S., & Patil, P. R. (2014). Carbon sequestration potential of tree species in the environment of North Maharashtra University Campus, Jalgaon (MS) India. *Bioscience Discovery, 5*(2), 175–179. http://biosciencediscovery.com

UNFCCC. (2008). *Kyoto Protocol reference manual*. United Nations Framework Convention on Climate Change. https://unfccc.int/sites/default/files/08_unfccc_kp_ref_manual.pdf

UNFCCC. (2015). *Conference of the Parties twenty-first session, adoption of the Paris Agreement*. https://doi.org/10.1007/BF0232712y

Vashum, K. T., & Jayakumar, S. (2012). Methods to estimate above-ground biomass and carbon stock in natural forests—a review. *Journal of Ecosystem & Ecography, 2*(1), 1–7.

Vicharnakorn, P., Shrestha, R. P., Nagai, M., Salam, A. P., & Kiratiprayoon, S. (2014). Carbon stock assessment using remote sensing and forest inventory data in Savannakhet, Lao PDR. *Remote Sensing, 6*(6), 5452–5479.

Wang, Z., Ma, Y., Chen, P., Yang, Y., Fu, H., Yang, F., … Ma, J. (2022). Estimation of rice aboveground biomass by combining canopy spectral reflectance and unmanned aerial vehicle-based red green blue imagery data. *Frontiers in Plant Science, 13*, 903643.

Xue, J., & Su, B. (2017). Significant remote sensing vegetation indices: A review of developments and applications. *Journal of Sensors, 2017*, 1353691. https://doi.org/10.1155/2017/1353691

Zhang, Y., Liang, S., & Yang, L. (2019). A review of regional and global scale biomass mapping. *Remote Sensing, 11*(23), 2744. https://doi.org/10.3390/rs11232744

Zhao, P., Lu, D., Wang, G., Wu, C., Huang, Y., & Yu, S. (2016). Examining spectral reflectance saturation in Landsat imagery and corresponding solutions to improve forest aboveground biomass estimation. *Remote Sensing, 8*(6), Article 6. https://doi.org/10.3390/rs8060469

Zheng, D., Rademacher, J., Chen, J., Crow, T., Bresee, M., Le Moine, J., & Ryu, S.-R. (2004). Estimating aboveground biomass using Landsat 7 ETM+ data across a managed landscape in northern Wisconsin, USA. *Remote Sensing of Environment, 93*(3), 402–411. https://doi.org/10.1016/j.rse.2004.08.008

Zheng, G., Chen, J. M., Tian, Q. J., Ju, W. M., & Xia, X. Q. (2007). Combining remote sensing imagery and forest age inventory for biomass mapping. *Journal of Environmental Management, 85*(3), 616–623. https://doi.org/10.1016/j.jenvman.2006.11.014

Zhu, X., & Liu, D. (2015). Improving forest aboveground biomass estimation using seasonal Landsat NDVI time-series. *ISPRS Journal of Photogrammetry and Remote Sensing, 102*, 222–231. https://doi.org/10.1016/j.isprsjprs.2014.08.014

Zhu, Y., Feng, Z., Lu, J., & Liu, J. (2020). Estimation of forest biomass in Beijing (China) using multisource remote sensing and forest inventory data. *Forests, 11*(2), 163. https://doi.org/10.3390/f11020163

Appendix

Appendix 1: Satellite data date and ID

Data Source	Year	Data date	Landsat_ID
Landsat 5	2005	24-Mar	LT05_L2SP_142041_20050324_20200902_02_T1
Landsat 5		3-Nov	LT05_L2SP_142041_20051103_20200901_02_T1
Landsat 5	2010	31-Mar	LT05_L2SP_141041_20100331_20200825_02_T1
Landsat 5		1-Nov	LT05_L2SP_142041_20101101_20200823_02_T1
Landsat 8	2013	21-Mar	LC08_L2SP_142041_20130321_20200913_02_T1
Landsat 8		18-Nov	LC08_L2SP_141041_20131118_20200912_02_T1
Landsat 8	2016	22-Mar	LC08_L2SP_142041_20160322_20200907_02_T1
Landsat 8		1-Nov	LC08_L2SP_142041_20161101_20200905_02_T1
Landsat 8	2025	15-Mar	LC08_L2SP_142041_20250315_20250326_02_T1

Appendix 2: Wood specific density of all species

LocalName	ScientificName	wood density
Amala	Phyllanthus emblica	0.8
Amba	Psidium guava	0.63
Angeri	Acacia pennata	0.55
Archal	Antidesma diandrum	0.59
Asare	Murraya koenigii	0.58
Badahar	Artocarpus lacucha	0.53
Bamboo	Bambusa spp.	0.65
Barkaule	Casearia graveolens	0.72
Barro	Terminalia bellirica	0.72
Bel	Aegal marmelosa	0.75

Bhalayo	Semecarpus anacardium	0.64
Bohori	Ehretia laevis	0.54
Botdhairo	Lagerstroemia parviflora	0.62
Botdhairo	Woodfordia fruticosa	0.59
Chilaune	Schima wallichii	0.73
Dumrai	Zizyphus rugosa	0.68
Guheli	Callicarpa arborea	0.62
Gutel	Trewia nudiflora	0.42
Harro	Terminalia chebula	0.96
Jamun	Syzygium cumini	0.85
Kaiyo	Myrsine sp.	0.61
Kapok	Ceiba pentandra	0.23
Karauta	Mellusa velutina	0.52
Karma	Adina cordifolia	0.59
Khayer	Acacia catechu	0.88
Khirro	Sapium insigne	0.47
Kumbhi	Careya arborea	0.62
Kusum	Schleichera trijuga/oleosa	0.96
Kyamuna	Cleistocalyx operculatus	0.66
Latikath	Glochidion acuminatum	0.45
MainKanda	Xeromphis spinosa	0.68
Padke	Albizia lucida	0.48
Putali kath	Casearia illiptica/elliptica	0.65
Rajbrikhsa	Cassia fistula	0.71
Sal	Shorea robusta	0.88
Saj	Terminalia alata	0.95
Sandan	Oujenia oojeinensis	0.89
Sani/Piyari Bhalayo	Buchannaia latifolia	0.45
Simal	Bombax ceiba	0.33
SimalKhair	Acacia auriculiformis	0.7
Sindhure	Mallotus philippensis	0.64
Sissoo	Dalbergia sissoo	0.78
Tatari	Dillenia pentagyna	0.53

Appendix 3: Correlation across different years and Seasons

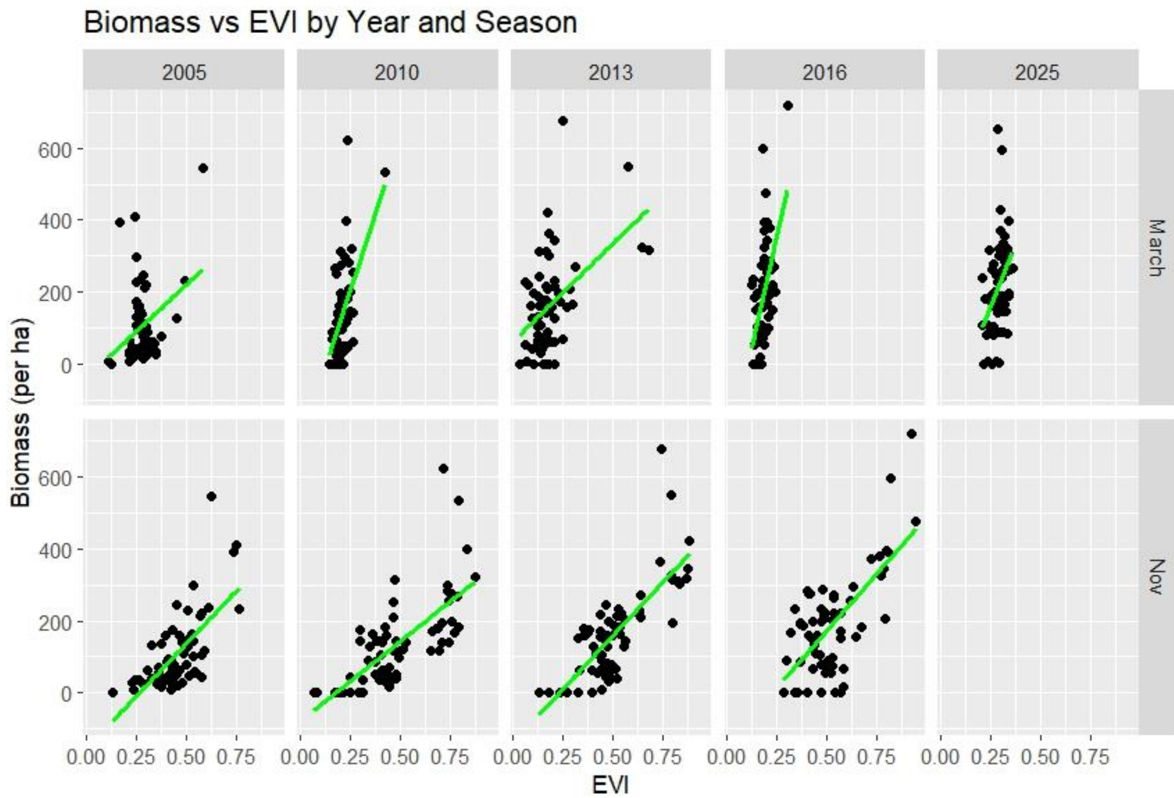

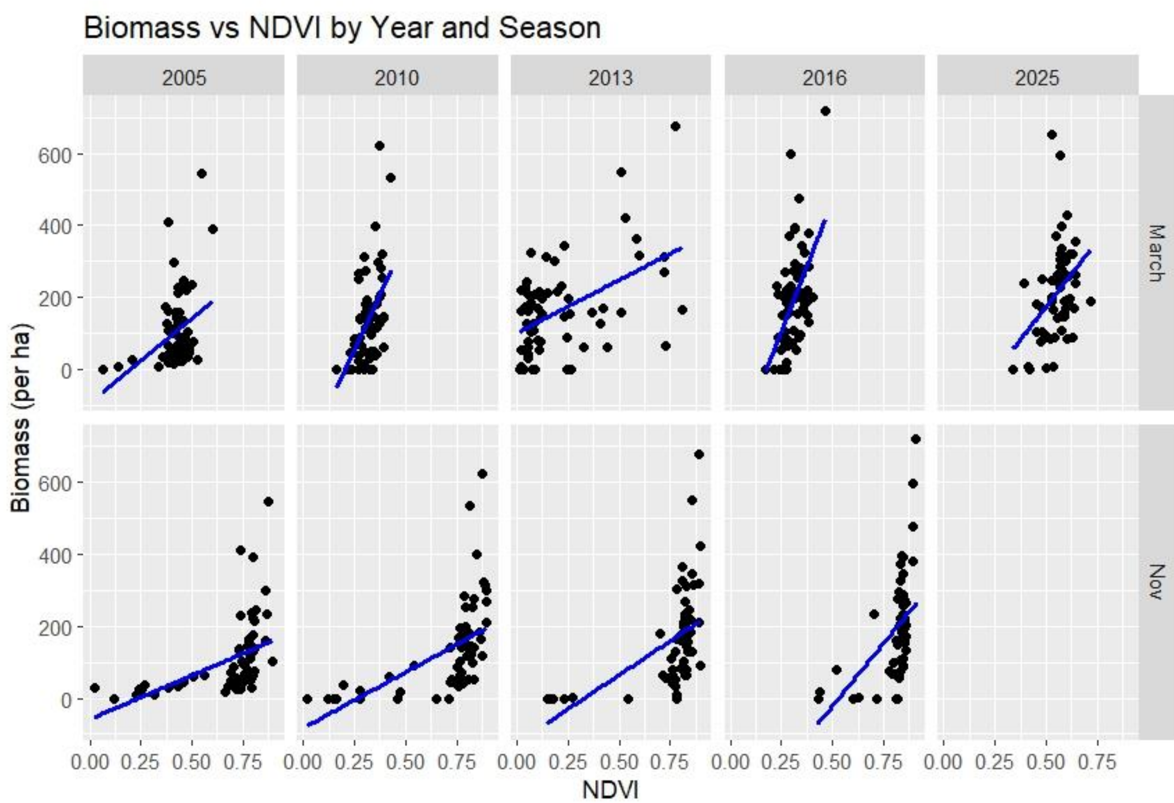

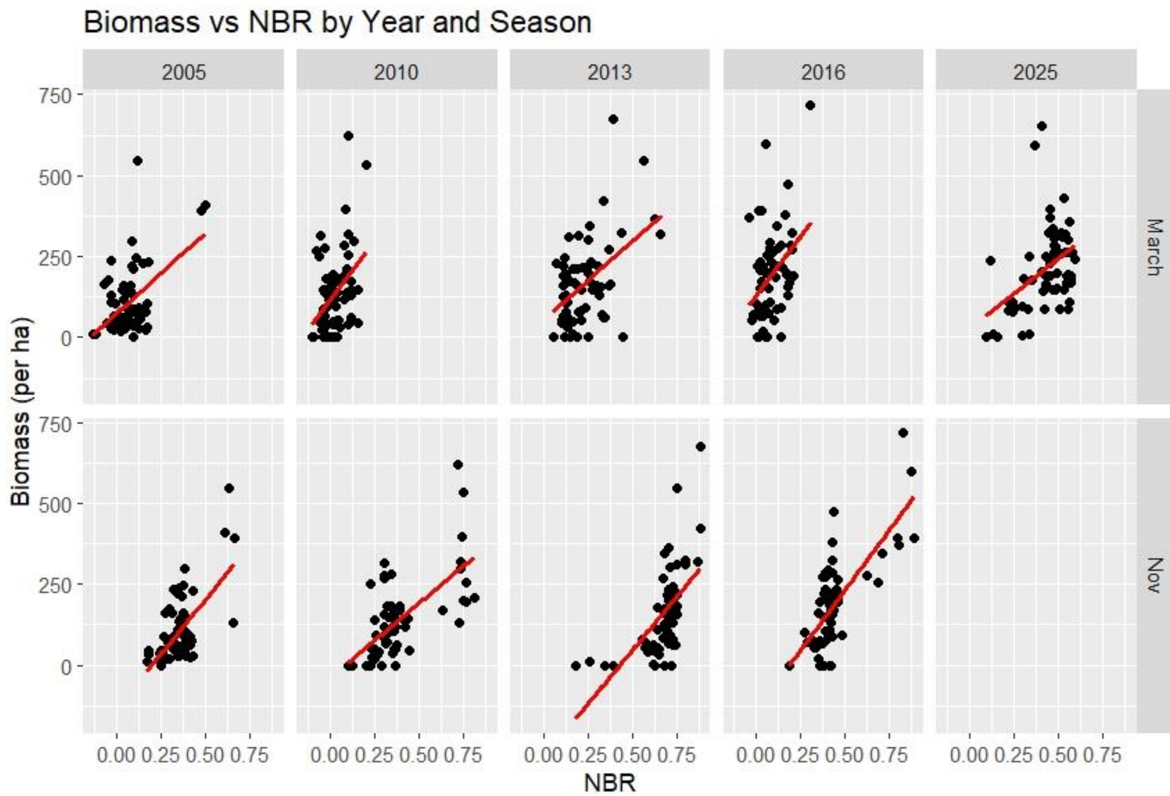

Appendix 4: Pearson correlation coefficient (r) of VIs across each year with p-values

Year	Season	VI	n	cor	p_value	conf_low	conf_high	se_z
2005	March	EVI	65	0.343384	0.005041	0.109088	0.542262	0.127
2005	March	NBR	65	0.495539	2.70E-05	0.286235	0.659705	0.127
2005	March	NDVI	65	0.359775	0.003245	0.127022	0.554976	0.127
2005	Nov	EVI	65	0.672156	8.75E-10	0.512232	0.787031	0.127
2005	Nov	NBR	65	0.612549	5.87E-08	0.433401	0.745127	0.127
2005	Nov	NDVI	65	0.471432	7.37E-05	0.257094	0.641563	0.127
2010	March	EVI	65	0.534984	4.41E-06	0.334766	0.688983	0.127
2010	March	NBR	65	0.40371	8.54E-04	0.177265	0.589558	0.127
2010	March	NDVI	65	0.487026	3.89E-05	0.2759	0.65332	0.127
2010	Nov	EVI	65	0.701402	7.65E-11	0.551922	0.807211	0.127
2010	Nov	NBR	65	0.660525	2.14E-09	0.496634	0.778936	0.127

2010	Nov	NDVI	65	0.537407	3.91E-06	0.337782	0.690765	0.127
2013	March	EVI	65	0.474434	6.53E-05	0.260703	0.643833	0.127
2013	March	NBR	65	0.47901	5.42E-05	0.266213	0.647287	0.127
2013	March	NDVI	65	0.492875	3.03E-05	0.282996	0.65771	0.127
2013	Nov	EVI	65	0.769224	7.17E-14	0.646645	0.853076	0.127
2013	Nov	NBR	65	0.60486	9.48E-08	0.423427	0.739643	0.127
2013	Nov	NDVI	65	0.499722	2.25E-05	0.291332	0.662834	0.127
2016	March	EVI	65	0.554737	1.63E-06	0.359475	0.703459	0.127
2016	March	NBR	65	0.377907	0.001912	0.147614	0.569331	0.127
2016	March	NDVI	65	0.543611	2.87E-06	0.345524	0.695321	0.127
2016	Nov	EVI	65	0.676117	6.39E-10	0.517568	0.789779	0.127
2016	Nov	NBR	65	0.730307	5.07E-12	0.591825	0.826915	0.127
2016	Nov	NDVI	65	0.517225	1.03E-05	0.312784	0.675864	0.127
2025	March	EVI	67	0.393673	9.81E-04	0.169493	0.579119	0.125
2025	March	NBR	67	0.431296	2.68E-04	0.213173	0.608467	0.125
2025	March	NDVI	67	0.387207	0.001208	0.162073	0.574026	0.125

Appendix 5: equation, its SE, and p-value of all models

A1: standard error and p-value for scenario 1

Quadratic Model:

$$y = -4.51 + 9.4308 \cdot NDVI\_March - 14.8264 \cdot NDVI\_Nov + 15.5571 \cdot EVI\_March - 3.7728 \cdot EVI\_Nov - 2.4495 \cdot NBR\_March + 16.4364 \cdot NBR\_Nov - 9.8222 \cdot NDVI\_March^2 + 25.095 \cdot NDVI\_Nov^2 - 11.553 \cdot EVI\_March^2 + 13.9201 \cdot EVI\_Nov^2 - 2.2245 \cdot NBR\_March^2 - 8.3856 \cdot NBR\_Nov^2$$

Model	Index	Term	Estimate	Std. Error	p-value
Linear	NDVI	March	4.0186	1.9638	0.042
Linear	NDVI	Nov	9.6338	1.3913	5.77E-11
Linear	EVI	March	6.4653	3.3073	0.0519

Linear	EVI	Nov	13.4186	1.6725	8.41E-14
Linear	NBR	March	-3.4718	2.4715	0.1617
Linear	NBR	Nov	8.2128	1.7274	3.79E-06
Quadratic	NDVI	March	9.4308	5.9374	0.1138
Quadratic	NDVI	Nov	-14.8264	6.1468	0.0168
Quadratic	$NDVI^2$	March	-9.8222	7.6671	0.2017
Quadratic	$NDVI^2$	Nov	25.095	5.8156	2.53E-05
Quadratic	EVI	March	15.5571	12.8363	0.227
Quadratic	EVI	Nov	-3.7728	7.2124	0.6015
Quadratic	EVI^2	March	-11.553	18.9428	0.5426
Quadratic	EVI^2	Nov	13.9201	6.3975	0.0308
Quadratic	NBR	March	-2.4495	4.4053	0.5788
Quadratic	NBR	Nov	16.4364	9.0561	0.0711
Quadratic	NBR^2	March	-2.2245	10.8709	0.8381
Quadratic	NBR^2	Nov	-8.3856	8.373	0.3178

A2: Standard Errors and p-values for Scenario 2- November VIs only

Quadratic Model:

$y = -0.0357 - 13.7512*NDVI\_Nov + 0.7426*EVI\_Nov + 9.79*NBR\_Nov + 24.5247*NDVI\_Nov^2 + 11.9481*EVI\_Nov^2 - 5.5042*NBR\_Nov^2$

Model	Index	Term	Estimate	Std. Error	p-value
Linear	NDVI	Nov	9.9	1.4212	4.40E-11
Linear	EVI	Nov	15.2865	1.6584	3.84E-17
Linear	NBR	Nov	5.6357	1.3705	5.68E-05

Quadratic	NDVI	Nov	-13.7512	6.4251	0.0335
Quadratic	$NDVI^2$	Nov	24.5247	6.0585	7.37E-05
Quadratic	EVI	Nov	0.7426	7.3525	0.9196
Quadratic	EVI^2	Nov	11.9481	6.5347	0.0689
Quadratic	NBR	Nov	9.79	8.3671	0.117
Quadratic	NBR^2	Nov	-5.5042	7.9658	0.491

A3: Standard Errors and p-values for Scenario 2- March VIs only

Quadratic Model:

$y = 5.9745 + 27.6339*NDVI\_March - 18.7554*EVI\_March + 25.9788*NBR\_March - 31.4234*NDVI\_March^2 + 42.9603*EVI\_March^2 - 34.503*NBR\_March^2$

Model	Index	Term	Estimate	Std. Error	p-value
Linear	NDVI	March	4.8522	3.1295	0.1226
Linear	EVI	March	7.7695	5.5435	0.1626
Linear	NBR	March	12.2235	3.2728	2.44E-04
Quadratic	NDVI	March	27.6339	9.396	0.0037
Quadratic	$NDVI^2$	March	-31.4234	12.5484	0.0131
Quadratic	EVI	March	-18.7554	22.2269	0.3998
Quadratic	EVI^2	March	42.9603	32.8935	0.193
Quadratic	NBR	March	25.9788	6.319	5.73E-05
Quadratic	NBR^2	March	-34.503	17.4454	0.0493

A4: Standard Errors and p-values for Scenario 2- March VI only with 2025 data

Quadratic Model:

$y = 104.0185 + 451.9122*NDVI\_March - 745.0697*EVI\_March + 454.6285*NBR\_March - 361.101*NDVI\_March^2 + 1281.6518*EVI\_March^2 - 286.8011*NBR\_March^2$

Model	Index	Term	Estimate	Std. Error	p-value
Linear	NDVI	March	115.6402	63.6644	0.0705
Linear	EVI	March	122.9607	114.3103	0.2831
Linear	NBR	March	355.0031	61.1755	1.92E-08
Quadratic	NDVI	March	451.9122	194.5735	0.021
Quadratic	$NDVI^2$	March	-361.101	252.4721	0.1539
Quadratic	EVI	March	-745.07	452.4114	0.1008
Quadratic	EVI^2	March	1281.652	653.01	0.0508
Quadratic	NBR	March	454.6285	126.3591	3.86E-04
Quadratic	NBR^2	March	-286.801	306.7868	0.3508

Appendix 6: Residual diagnostics

Scenario 1- Linear residual vs fitted

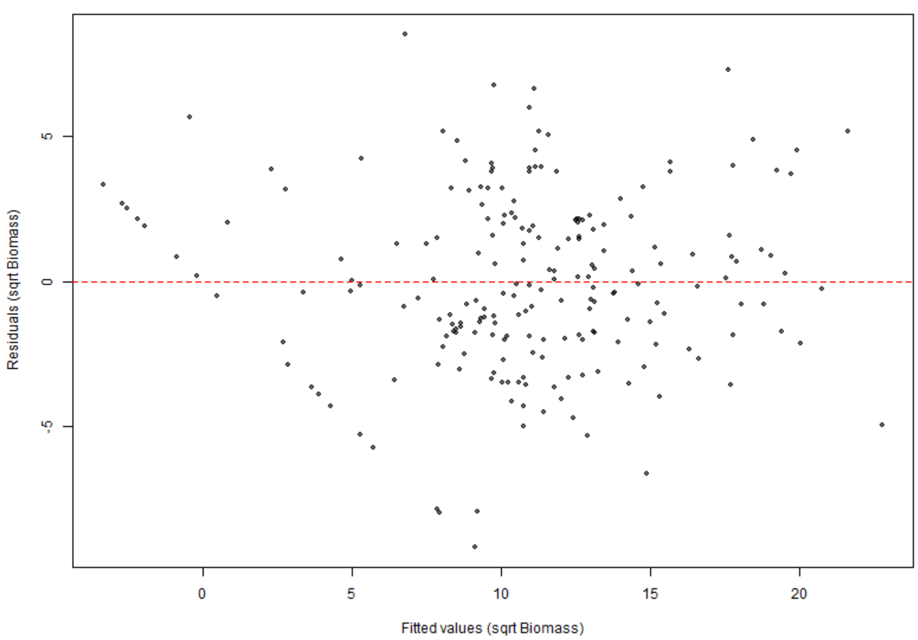

Scenario 1- Quadratic residual vs fitted

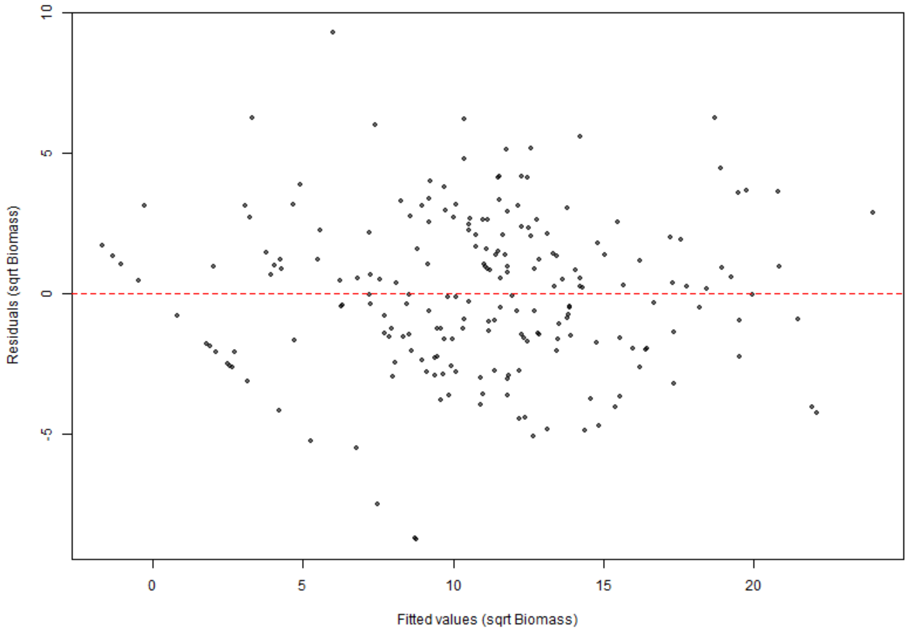

Scenario 1- Random residual vs fitted

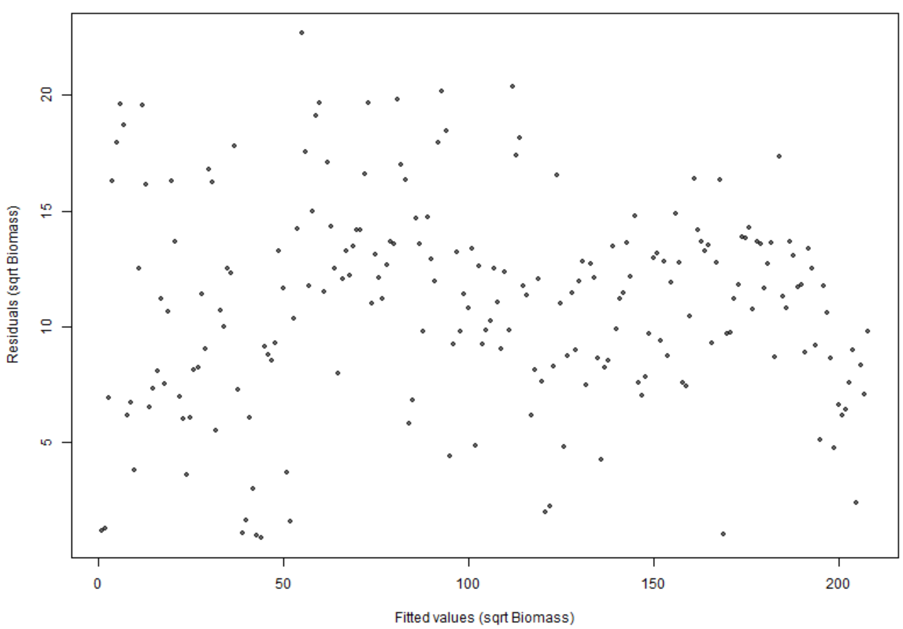

Scenario 2- Linear residual vs fitted (Nov only)

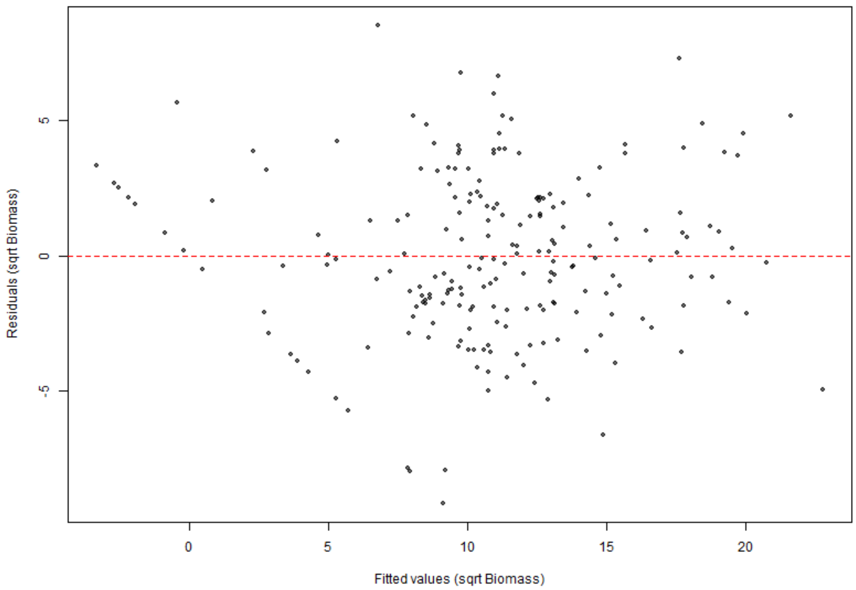

Scenario 2- Quadratic residual vs fitted (Nov only)

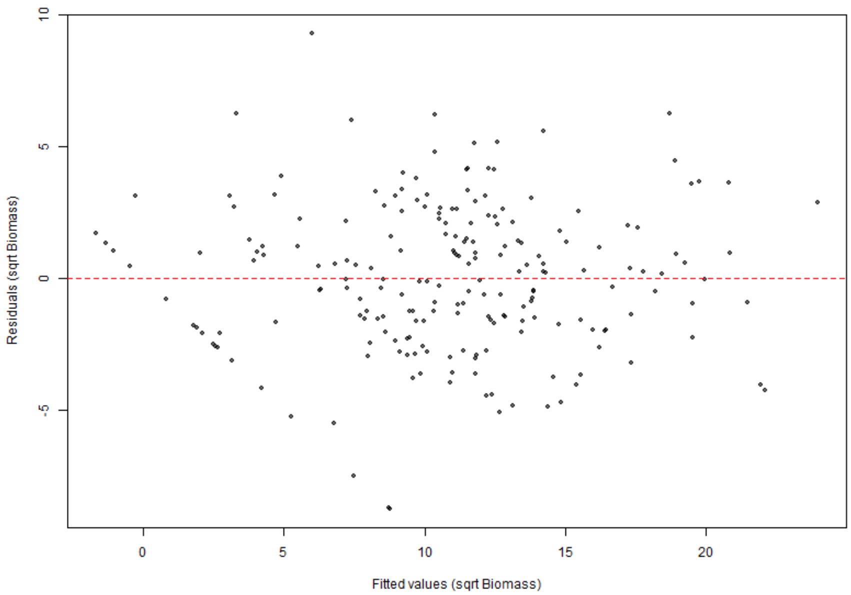

Scenario 2- Random residual vs fitted (Nov only)

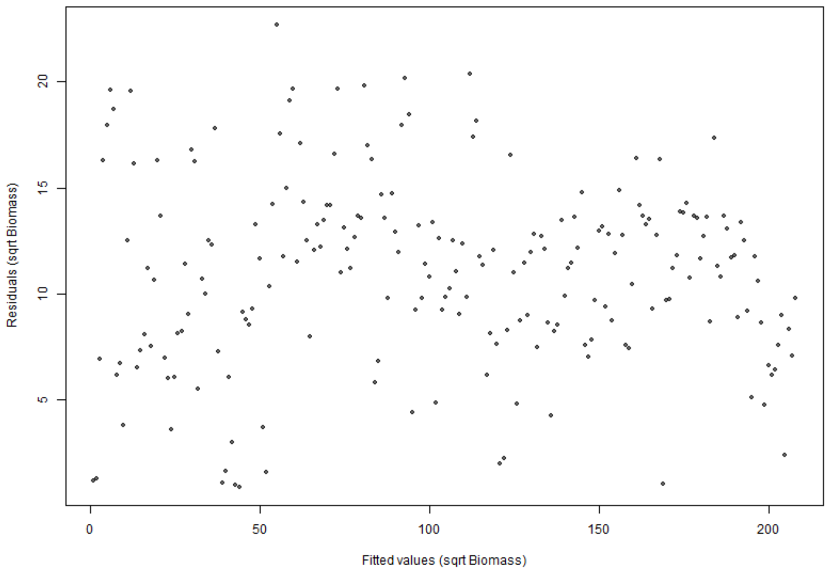

Scenario 2- Linear residual vs fitted (March only)

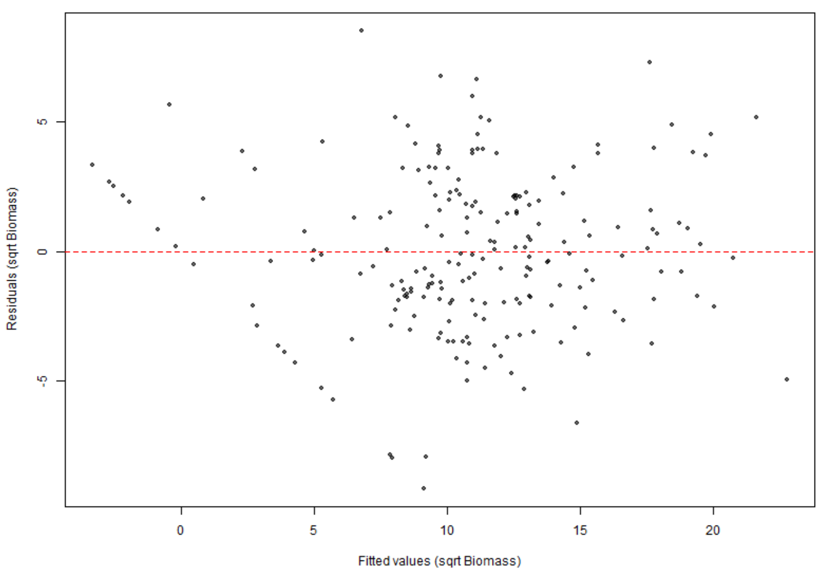

Scenario 2- Quadratic residual vs fitted (March Only)

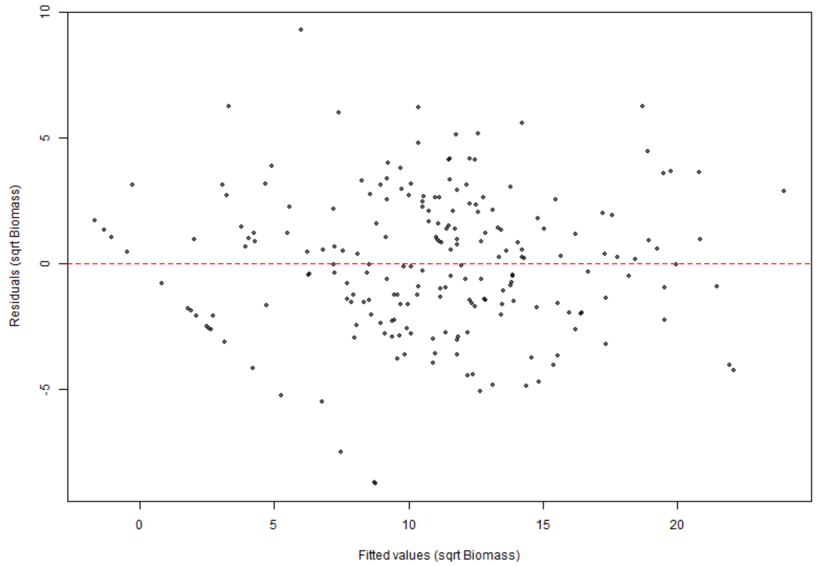

Scenario 2- Random residual vs fitted (March only)

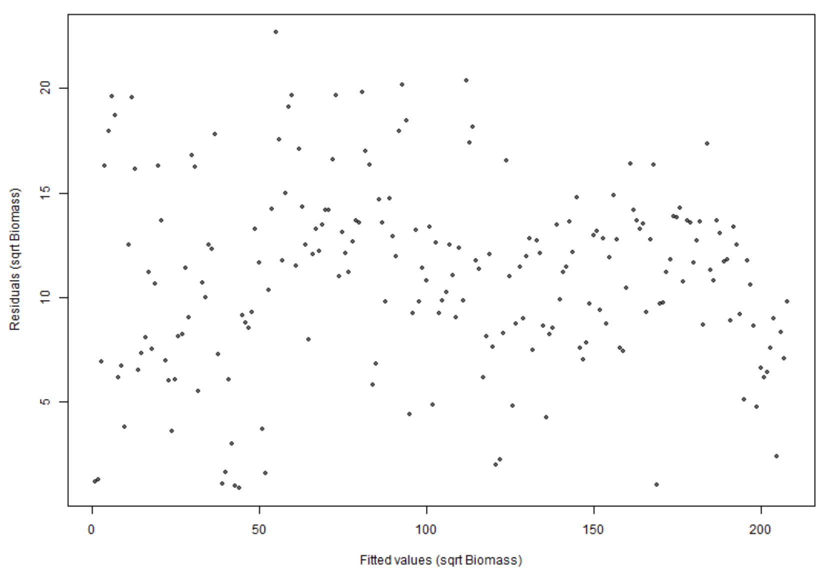

Scenario 2- Linear residual vs fitted (March only with 2025 data)

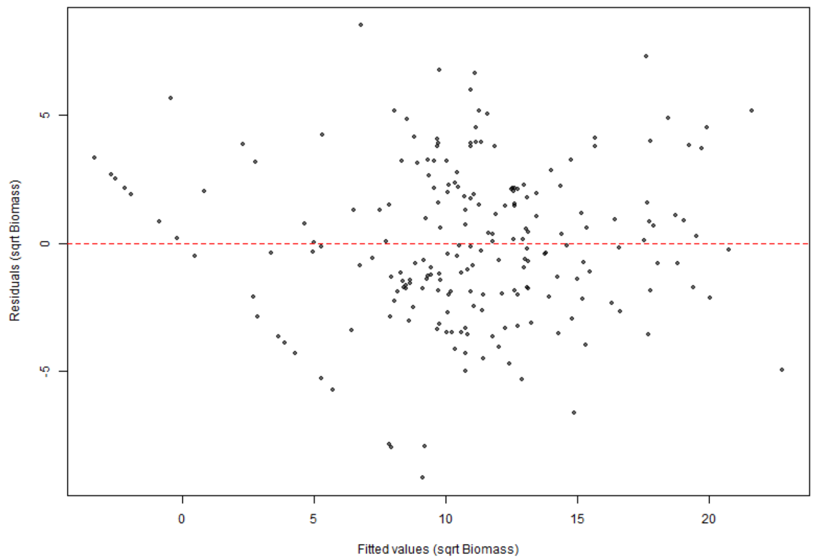

Scenario 2- Quadratic residual vs fitted (March only with 2025 data)

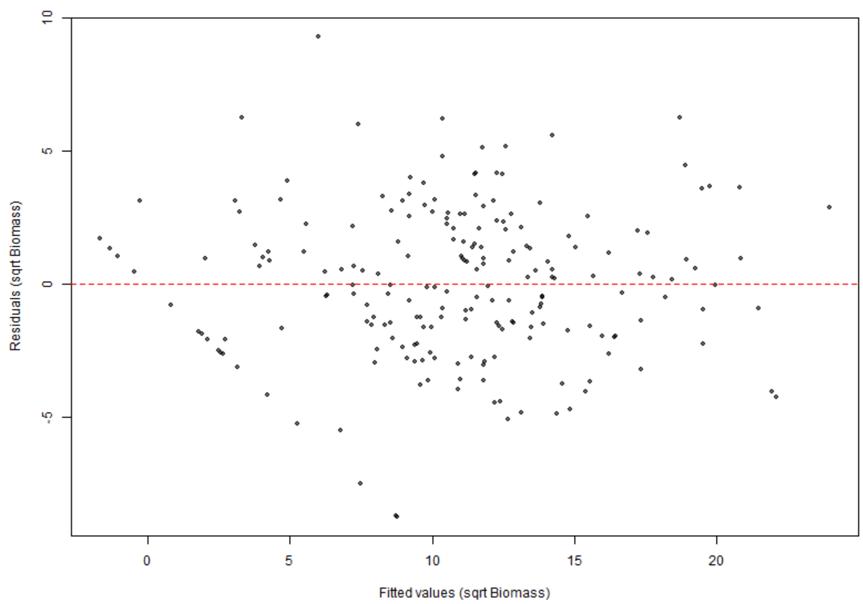

Scenario 2- Random residual vs fitted (March only with 2025 data)

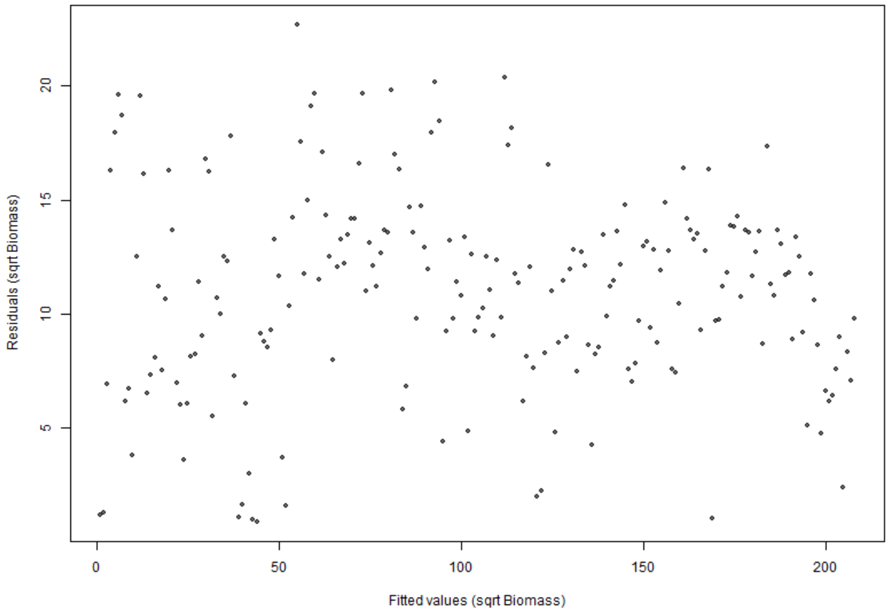

Scenario 3- Linear residual vs fitted (Elevation and weather data)